# Shaft Assembly Design and Fabrication for FSAE Engine Dynamometers

Pranaya Pokharel[a*], Jesse Green[b], Theron Honore[b], and Elias Tezaguic[b]

[a] *Assistant Professor, McCoy School of Engineering, Midwestern State University, Wichita Falls, TX, USA*

[b] *Student, McCoy School of Engineering, Midwestern State University, Wichita Falls, TX, USA*

*****Corresponding author, email: pranaya.pokharel@msutexas.edu

**Abstract:**

Dynamometers, commonly referred to as dynos, are indispensable tools in validating automotive design concepts. This study focuses on testing engines with a displacement of 710cc or less, aligning with Formula Society of Automotive Engineers (FSAE) guidelines. The dynamometer design incorporates features like vibration reduction mechanisms and customized Arduino code to simulate one FSAE driving scenario: steady state driving. At the core of the dynamometer's operation is an eddy current brake powered by an AC source, employing Faraday's Law of electromagnetic induction to mimic dynamic resistance. Engine power is transmitted to the eddy current brake through a meticulously analyzed shaft, engineered to withstand torques of up to 65 Nm. The dynamometer's design emphasizes modularity, facilitated by adjustable front and rear mounts securely fastened with bolts and nuts. The frame is built to house electrical components and adjustable mounting regions to connect the eddy current brake with the engine via the designed shaft. Once operational, our engine dynamometer will serve as a valuable tool for monitoring various engine parameters, including power output, torque, engine speed, fuel consumption, exhaust gas composition, as well as coolant and oil temperatures. This comprehensive data collection will significantly aid in evaluating engine performance under various FSAE driving conditions.

# 1 Introduction:

## 1.1 Motivation

In January 2021, Midwestern State University established its Formula Society of Automotive Engineers (FSAE) team, marking the beginning of an exciting journey. FSAE, a renowned student design competition, draws participation from over a hundred schools nationwide and internationally. The challenge involves the creation of formula-style race cars, putting schools against each other in a test of teamwork and engineering prowess. The inaugural race car, crafted by our team in May 2022, faced a significant hurdle during development.

The absence of a testing facility at our school meant that critical components designed by sub-teams, such as powertrain, drivetrain, electronics, and suspension, could only be evaluated while the car was in motion. Live testing became the sole method for collecting data on engine performance, tire functionality, and sensor operations, leading to uncertainties about component reliability until the competition neared.

In response to this challenge, the FSAE team convened on August 24, 2022, with a shared determination to address the issue. The solution: the design and construction of an engine dynamometer (dyno). Dynamometers are instrumental in measuring torque, rotational speed, emissions, and simulating specific driving conditions. This innovative system will empower our team to conduct comprehensive tests, optimizing engine performance, sensor functionality, tire efficiency, and refining power transmission to the drivetrain.

The project, inherited from the 2022-2023 group [1], initiated modular designs and accumulated materials for completion. Over a 28-week period, evenly split between the fall and spring semesters, our team built upon the foundation laid by its predecessors. The focus is on finalizing the structural framework while catering ways to mitigate vibration. The secondary focus is on installing electrical components and ensuring the seamless transfer of power from the engine to the eddy current brake. Robust data acquisition systems will be implemented for accurate sensor readings.

Dynamometers are useful to test the engine performance for FSAE teams. Hence, their design is done by various FSAE teams globally [2]. This cost-effective dynamometer will cater to engines of 710cc and below, aligning with FSAE rules. Compliance with competition regulations, such as the requirement for a restrictor with a diameter no greater than 20 mm to limit power output, influenced the choice of the dyno. This project embodies our commitment to innovation, problem-solving, and elevating the capabilities of our FSAE team.

## 1.2 Background of the Dyno

Different types of braking systems have been used in dynamometers [6]. Water Brake Dynamometers are sometimes used for braking [3]. Current research in dynamometers includes both experimentation [4] and simulation aspects [5].

The chosen dynamometer for this project was the Eddy Current dyno so that the dynamic testing (variation of dynamic loads on the tires) could be done, operating on the principles of electromagnetic induction. In this system, electromagnetic force (emf) is generated by the displacement between conductors and a magnetic field. Consequently, the motor experiences a counterforce that seeks to decrease the engine's output revolutions per minute (rpm).

Opting for the Eddy Current dyno offered several advantages, including a streamlined and easily assembled construction, a robust power-handling capacity, heightened responsiveness to

changes in input signals, an extended operational lifespan, and simplified maintenance requirements due to its minimalistic components. However, it comes with certain drawbacks, such as the inability to produce torque at zero speed and a relatively compact size, which diminishes its strength and reliability.

After a thorough exploration of various dyno setups, the previous team deliberated and ultimately chose the Eddy Brake configuration for the engine dyno [1]. This decision was driven by the Eddy Current dyno's ability to meet all the specified project requirements.

A dynamometer, also called a dyno, is a tool used to monitor and evaluate an engine's performance characteristics in a controlled environment. It is an essential tool for engine development, testing, and optimization for a variety of uses, such as industrial, automotive, and aerospace machinery. An engine dynamometer is primarily used by engineers to measure and analyze important metrics including power output, torque, fuel consumption, emissions, and overall efficiency by simulating and assessing the engine's behavior in a controlled environment. An instrument for data acquisition, control systems, and a loading mechanism are some of the parts that make up an engine dynamometer. In order to simulate the forces an engine would encounter during actual operation; the loading device delivers a resistance or load to the engine. This makes it possible to measure how well the engine performs under various operating circumstances, such as varied loads, speeds, and temperatures.

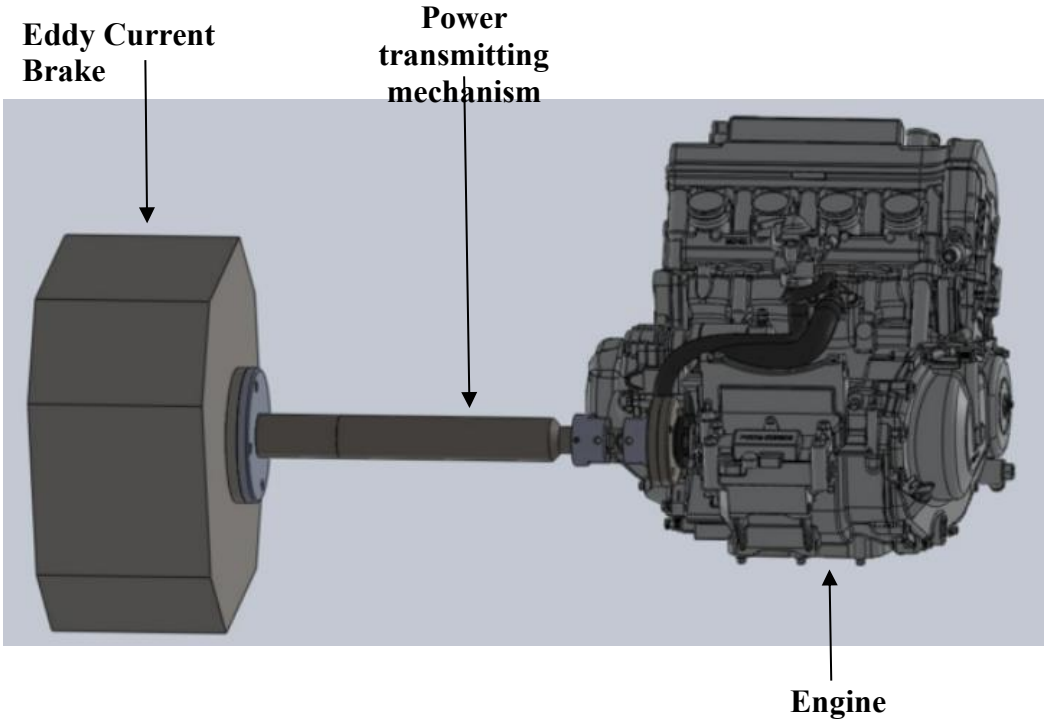


*Figure 1: Engine Dynamometer Assembly*

The assembly in figure 1 illustrates the loading mechanism (left), the power transmitting shaft (in the middle), and the current 2002 Honda CBR600 f4i engine that is on the 2024 FSAE car (right). The loading mechanism we will be using is an eddy current brake.

An eddy current brake is a kind of electromagnetic braking device that slows down or stops a moving object by creating a resistive force using the concepts of electromagnetic induction [7]. The generation of eddy currents, or circulating currents induced in a conductor, in response to variations in magnetic flux is the fundamental principle of an eddy current brake. This phenomenon is related to electromagnetic induction according to Faraday's Law.

The paper is the outcome of the work done for the Senior Design Project, which is a year-long capstone project for Mechanical Engineering Curriculum at MSU Texas. The ideas of the shaft design and finishing fabrication is the group's own creative and innovative effort. The paper is organized in different sections. Section 2 discusses the methods used during the project. Section 3 describes the design aspects and description. Section 4 highlights the outcome and results of the project followed by conclusions in Section 5.

## 2 Method:

### 2.1 Concept:

Initially, the group was tasked with understanding the principles of the eddy brake to be used for the dynamometer.

The eddy current brake system operates on the principles of electromagnetic induction and eddy current generation, offering a non-contact method for applying controlled resistance to a rotating object. In our engine dynamometer project, the theoretical foundation of the eddy current brake system played a crucial role in achieving precise control over the braking force applied to the engine.

### 2.2 Eddy current brake principles

The foundation of our eddy current brake system lies in the principles of electromagnetic induction, as described by Faraday's law. According to Faraday's law, the electromotive force (EMF) induced in a closed loop is directly proportional to the rate of change of magnetic flux through the loop (Figure 2) [8]. This relationship is expressed as:

$$\varepsilon = -N\frac{\Delta\phi}{\Delta t} \quad \text{..... (1)}$$

Where: $\varepsilon \rightarrow$ the induced electromotive force

$\Phi \rightarrow$ the magnetic flux

$t \rightarrow$ time

$N \rightarrow$the number of turns (coil wires)

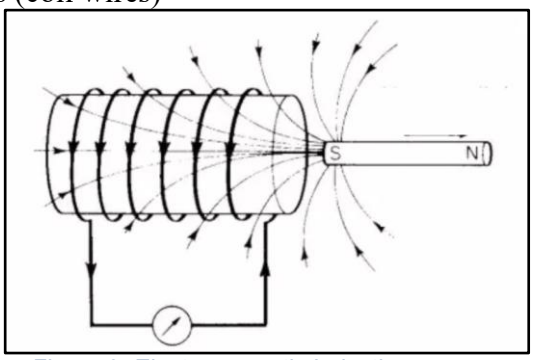


*Figure 2: Electromagnetic Induction*

The system leverages electromagnetic induction to generate eddy currents within a conductive surface. When a magnetic field, produced by coils surrounding the braking surface, interacts with the rotating object (conductive surface), it induces circulating currents, known as eddy currents, within the material [9]. The eddy currents, in turn, create their own magnetic field, opposing the original magnetic field that induced them (Figure 3). This opposition generates a resistive force, providing a controlled braking effect on the rotating object. The strength of the braking force.

The magnetic field generated by the coils in our eddy current brake system is fundamental to the induction of eddy currents (Figure 4) [10]. The strength of the magnetic field ($B$) is directly related to the number of turns in the coil ($N$), the current flowing through the coil ($I$), and the coil's magnetic permeability (μ):

$$B = \frac{\mu \cdot N \cdot I}{2 \cdot \pi \cdot r} \quad \text{..... (2)}$$

Where: $B \rightarrow$ the magnetic field strength

$\mu \rightarrow$ the magnetic permeability ($4\pi \times 10^{-7} Tm/A$)

$N \rightarrow$ the number of turns in the coil

$I \rightarrow$ the current of the flowing through the coil

$r \rightarrow$ the distance from the center of the coil

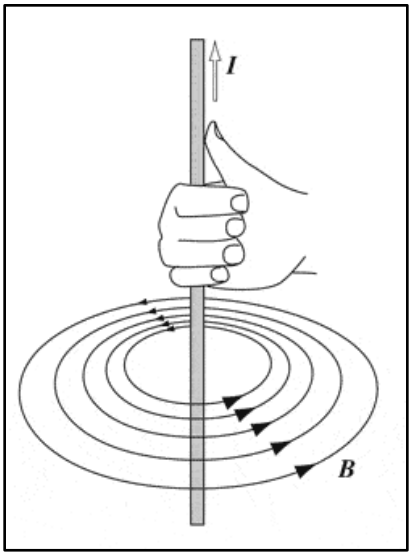


*Figure 3: Magnetic Field Strength [17]*

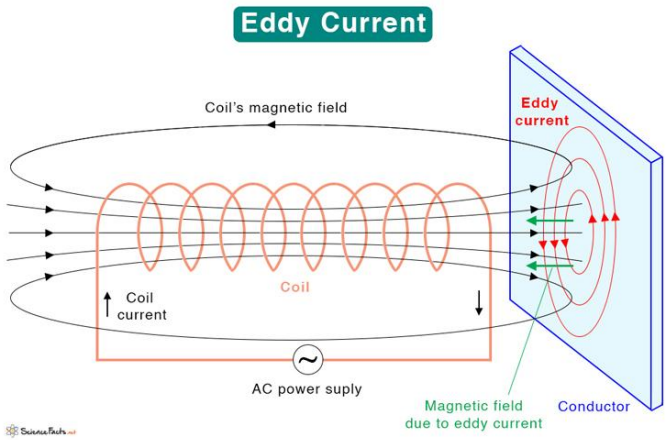


*Figure 4: Coil Operational Diagram [10]*

The magnetic flux ($\Phi$) through a closed loop is determined by the product of the magnetic field strength and the perpendicular area through which the field lines pass,

$\Phi = B \cdot A$ ..... (3)

Where: A → surface area

Lenz's law is based on the principles of conservation of energy and Newton's 3rd law [11]. This was the most convenient method to determine the direction of the induced current. This law states that the induced electromotive force with different polarities induces a current whose magnetic field opposes the change in magnetic flux through the loop in order to ensure that the original flux is maintained through the loop when current flows in it. In other words when there is a change in the magnetic field through a conductor, it induces an electromotive force (EMF) that generates an electric current. This induced current creates a magnetic field that opposes the change in the original magnetic field. For example, imagine you have a wire, and you're moving a magnet near it. Lenz's Law says that if this moving magnet creates an electric current in the wire, the direction of that current will be such that it will try to stop the magnet from moving.

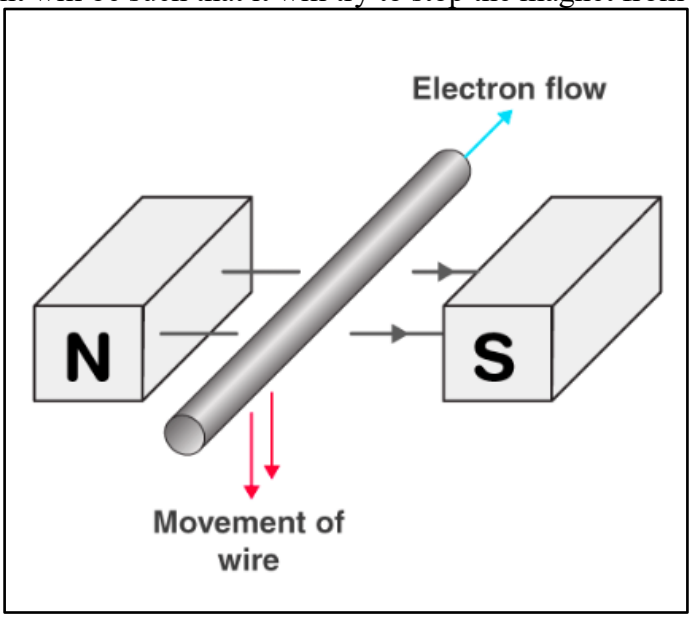


*Figure 5: Lenz's Law [11]*

The incorporation of fundamental electromagnetics principles into the design of our eddy current brake system establishes a theoretical foundation that aligns seamlessly with the dynamic testing requirements of our engine dynamometer. The utilization of Faraday's law ensures that the electromotive force is induced by the changing magnetic flux provides precise control over the eddy currents, this allows us to modulate the braking force dynamically. The magnetic field strength, which depends on the coil turns, current and magnetic permeability, directly influences the intensity of the braking force. This relationship facilitates the fine-tuning necessary for simulating FSAE competition scenarios in engine dynamometer testing. The advantage of the non-contact braking is that Lenz's law ensures that the induced currents resist the changes in magnetic flux, providing a non-contact braking mechanism. This feature minimizes wear and tear, offering longevity and reliability in our engine dyno operations. Equation 4 below was critical for the interaction between a conductor and a magnetic field. It provided a quantitative relationship for the force experienced by the conductor with both the magnetic field strength and the speed at which the conductor cuts through the magnetic flux. This formula enabled us to identify factors that will affect the braking capacity of the eddy current brake.

$$F_d = \alpha\sigma\delta BAv \quad \text{..... (4)}$$

Where: $F_d$ = This is the force experienced by the conductor, measured in Newtons (N).
$B$ = This represents the magnetic field strength, measured in Tesla (T)
$A$ = This is the area of the conductor that is perpendicular to the magnetic field lines, measured in square meters ($m^2$).
$v$ = This is the velocity of the conductor perpendicular to the magnetic field lines, measured in meters per second (m/s).

### 2.2.1 AF50-90 Operating principle

When the electrical current flows from the stator into the coils with alternating polarity, it generates a magnetic field which closes through the rotors. This magnetic field generates eddy currents in the rotors, which counter revolutions and then decelerate the drive shaft. This effect is achieved through electromagnetic induction alone – with no contact, there is no wear. The Telma rotors rotate with the drive shaft, when electricity is sent to the coils to create alternating red north pole and blue south pole electromagnets [12].

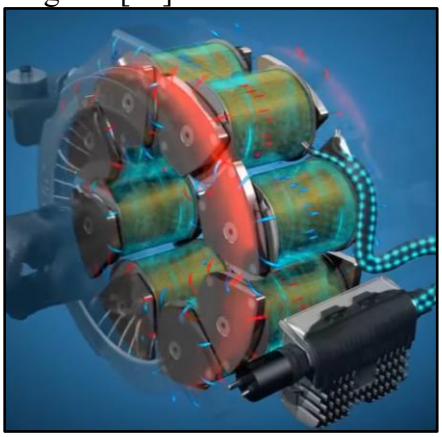

*Figure 6: Eddy Brake Operating Principle [12]*

### 2.2.2 Eddy brake (AF50-90 Retarder) Specifications

The eddy current brake that was selected by a group of senior students last year, was the Telma AF50-90 retarder. The Telma AF50-90 retarder is a commonly used electromagnetic brake in various trucks and larger automobiles, as well as in project dynamometers similar to this one. The total weight of the eddy brake is 223 lbs. or 101 kg, with this weight divided between the rotor (62 lbs. or 28 kg) and the stator (161 lbs. or 73 kg) which is the external housing. It is 363mm (14.15 in.) in height, 400mm (15.6 in.) in width, and 261mm (10.18 in.) in thickness. It is capable of 900 Nm (663 lb.-ft) of braking torque, 10,000 Nm (7,370 lb.-ft) maximum transmissible torque, and 4500 rpm maximum bearing speed [13-16].

### 2.2.3 Eddy brake configuration

The eddy current brake provides a braking power of 94 kW, providing the capability to exert substantial resistance against the rotational forces of the shaft. This braking power was essential to replicate FSAE simulation scenarios during our dynamic testing, ensuring the accuracy and reliability of our engine dyno performance analysis. The eddy brake operates at a voltage of 12 V as the standard configuration, optimizing the efficiency of the eddy current brake system. The resistance specifications can provide critical insights into the electrical characteristics. The resistance per coil and per circuit determines the impedance faced by the electrical current. The electrical current drawn per circuit is 49 A. This ensured optimal performance, striking a balance between the electrical power supplied and the braking force generated. The AF50-90 retarder features a four-stage configuration in parallel; each stage operates independently, providing a modular approach to tailoring resistance levels. The parallel configuration enhances the AF50-90's suitability for a diverse range of testing scenarios, allowing for independent control and adjustment of each stage. Additionally, a defining feature of the AF50-90 retarder is the two coils in parallel per stage. This strategic design helped the adaptability and responsiveness of the braking system. The parallel configuration optimizes the flow of the eddy current, providing an important and precisely adjustable braking system. Putting these aspects into perspective, we determined that the eddy current brake demands 12 V and a current of 196 A to provide braking power at its full capacity.

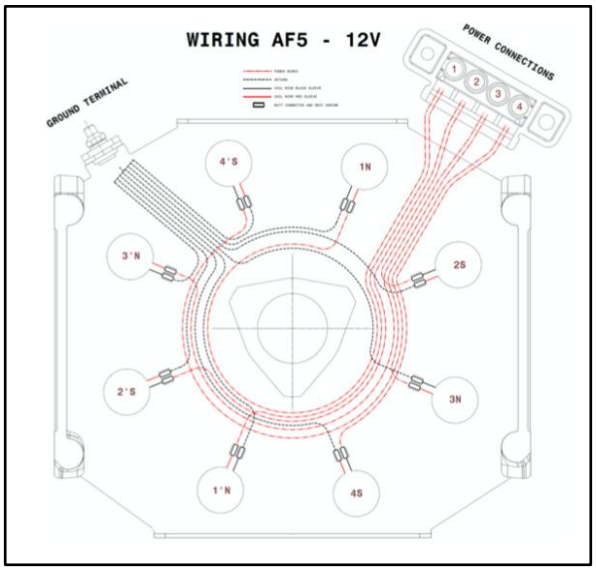


*Figure 7: Wiring Configuration in Parallel [13]*

## 3 - Apparatus Design and Description

### 3.1 - Shaft Design

A power-transmitting mechanism was one of our initial design considerations, whereby we assessed the viability of a chain drive and a shaft. A unanimous decision was made to use a shaft as the power-transmitting mechanism for the engine dynamometer, as we carefully considered various factors. One of the crucial considerations was the need to minimize power losses, and a shaft was deemed advantageous in this regard. Unlike a chain, a shaft provides a direct and rigid connection, reducing inherent flexibility that might result in energy absorption and dissipation, ultimately enhancing the efficiency of the system.

The evaluation also considered factors such as maintenance requirements, backlash, play, vibrations, and noise. While both shafts and chains share similarities in these aspects, the specific operational demands of the dynamometer favored the characteristics of a shaft. The reduced flexibility, potential for direct drive, and the ability to mitigate issues such as misalignment made a shaft-based system more suitable for achieving the precision and accuracy required for measurements.

Furthermore, the torque capacity of a shaft was recognized as advantageous in this application. The direct drive offered by a shaft between the engine and the eddy current brake contributed to a more power-efficient transmission, eliminating the need for additional components that might introduce inefficiencies into the system.

The decision to choose a shaft over a chain as the power-transmitting mechanism for the engine dynamometer was driven by a strategic alignment of design considerations, efficiency goals, and the specific operational requirements of the dynamometer setup. The decision reflects a holistic approach to optimizing performance and ensuring the reliability of the dynamometer system.

Having selected a shaft as the power-transmitting mechanism, the focus shifted to the design considerations for the shaft. Design was sought based on concepts from design literature [18, 19]. The shaft needed to accommodate attachment points for both the engine's drivetrain sprocket and

the rotor of the eddy current brake. The original design of the shaft assumed of a basic idea where the shaft is connected to 2 fixed points - one fixed point represents the engine and the other fixed point represents the eddy current brake. This provided a starting point for our design and eventually, several mechanical adaptors, including flanges and a double universal joint, were integrated to ensure complete and functional power transmission for any FSAE compliant engine. This was a primary asset to be considered as modularity is the key novelty in our design.

It is crucial to highlight that the inclusion of a double universal joint on the engine side was necessary to address potential misalignment between the engine and the eddy current brake. Additionally, a bearing, specifically a pillow block bearing, was essential. A pillow block bearing is a mounted unit comprising a bearing and a housing, typically constructed from materials like cast iron. This type of bearing is engineered to provide support and secure positioning for a rotating shaft. The pillow block bearing, in this case, is strategically positioned in close proximity to the eddy current brake.

Before dimensioning can take place for any of the aforementioned components, a diameter was required to be sized in order so that a torque can be safely transmitted from the engine to the eddy current brake. Chrome-plated 1045 steel was chosen as the potential material for the design of the shaft. Initial calculations were performed to obtain an approximate value, enabling subsequent in-depth analysis. Calculations were done to cater to three different scenarios, namely static conditions, fatigue conditions, and dynamic conditions.

Safety is the first priority in every engineering structure's design. When the team designed the shaft, we took ethics into account and made sure that the Factor of Safety (FOS) is at least 1.5. This decision is based on ethical principles that place a high priority on people's safety, well-being, and risk mitigation. This pledge is a recognition of the uncertainty present in practical applications.

Engineers who responsibly mitigate risk by incorporating a margin of safety into structural or component designs implement a factor of safety (FOS) that exceeds projected loads or stresses. Professional responsibility is essential, requiring engineers to adhere to industry standards and put public safety first. Following these guidelines guarantees legal and regulatory compliance, as many nations have minimal FOS requirements. It also fits with ethical engineering approaches.

Using a FOS of 1.5 promotes long-term sustainability and goes beyond short-term safety concerns. This is an ethical choice. This method reduces the possibility of early failures and, as a result, the environmental effect of repairs or replacements. By making engineers responsible for industry norms, the transparency in engineering procedures that results from this decision improves clear communication regarding safety levels in designs. The implementation of a FOS of 1.5 or higher represents, ethically speaking, a dedication to resilient, safe, and sustainable engineering solutions for the good of people and communities.

### 3.1.1 - Static Conditions:

The design replicates the shaft using a fixed beam, as illustrated in Figure 8. This approach is taken to emulate our envisioned shaft, which is intended to link directly from the engine to the eddy current brake. The utilization of fixed supported beams mirrors this requirement, ensuring that the shaft has both vertical and lateral restraints. This configuration helps alleviate any potential play in the shaft, thereby minimizing power losses.

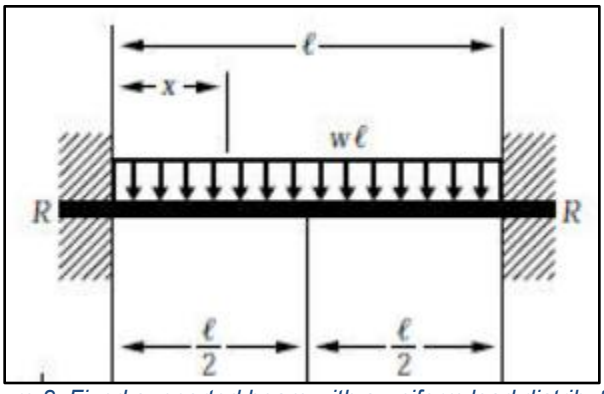


*Figure 8: Fixed supported beam with a uniform load distribution*

$$\delta_{max} = \frac{wl^4}{384EI} \quad \text{..... (5)}$$

Where: $\delta_{max}$ → the maximum deflection of the beam in meters (m)
w → the weight distribution per unit length in Newtons per meter (N/m)
l → length of the beam between both support points (18 inches = 0.4572 m)
E → Young's Modulus (Modulus of Elasticity) of chrome plated 1045 steel (206 GPa)
I → Area moment of Inertia in meters to the fourth ($m^4$)

$$I = \frac{\pi d^4}{64} \quad \text{..... (6)}$$

Equations can be rearranged to modify it for our specific needs. Firstly,

$$\text{Let } w = \frac{W}{l} = \frac{\rho V g}{l} = \frac{\rho A h g}{l} = \frac{\rho \frac{\pi d^2}{4} g l}{l} = \frac{\rho \pi d^2 g}{4} \quad \text{..... (7)}$$

Where: V → volume of space occupied by the beam
g → Gravitational field strength in Newtons per kilogram (N/kg)
A → Cross sectional area of shaft in square meters ($m^2$)
$\rho$ → Density of 1045 steel in kilogram per cubic meter (7861 kg/$m^3$)

$$\text{Recall that } I = \frac{\pi d^4}{64} \quad \text{..... (8)}$$

Substituting gives

$$\delta_{max} = \frac{\frac{\rho \pi d^2 g}{4L} \cdot l^4}{384E \cdot \frac{\pi d^4}{64}}$$

The above equation can be simplified to give

$$\delta_{max} = \frac{\rho g l^3}{384 E d^2}$$

Rearranging for the diameter 'd' gives the formula

$$d = \sqrt{\frac{\rho g l^3}{384E \cdot \delta_{max}}} \quad \text{..... (9)}$$

$$d = \sqrt{\frac{(7861)(9.8)(0.1778)^3}{384(206 \times 10^9)(0.001)}}$$

$$d = 7.399 \times 10^{-5}\ m\ = 0.002913\ in$$

The diameter value of 0.002913 inches is notably small, as anticipated. A shaft without external loading, apart from its own inherent weight, typically demands a less robust design. Nevertheless, conducting these calculations is crucial to establish a reliable starting point. It is reasonable to assume that this diameter represents the smallest value upon comparison with both fatigue and dynamic conditions, justifying its selection in our analysis.

### 3.1.2 - Fatigue Conditions:

The subsequent investigation focused on designing a shaft capable of withstanding fatigue. Fatigue, characterized by the development of cracks in materials and structural components due to cyclic (or fluctuating) stress, poses a critical consideration. When a shaft is set in rotation, it encounters varying bending moments and torques in different regions, depending on its rotary position. To determine the appropriate diameter, the DE - Goodman criteria was employed. Representing the second most conservative approach for fatigue analysis in shafts, as depicted in Figure 9, the Goodman criterion is widely utilized. It strikes a balance between complexity and accuracy, rendering it practical for routine fatigue assessments. Once the associated points, comprising alternating stress and mean stress, are identified, the material is expected to endure an infinite life under such a combination of cyclic loads.

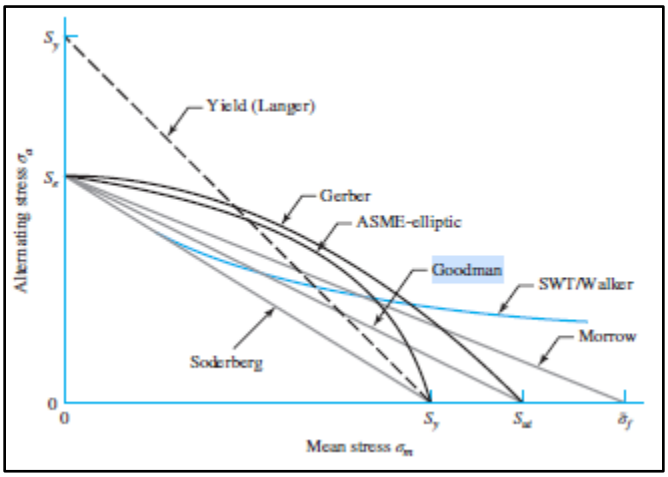


*Figure 9: Generic graph of alternating stress against mean stress highlighting the different criteria*

The Goodman criteria is highlighted in blue and it can be seen to be the second most conservative criteria.

The general formula that governs the relation is as follows:

$$\frac{\sigma_a'}{S_e} + \frac{\sigma_m'}{S_{ut}} = \frac{1}{n} \quad \text{..... (10)}$$

Where: $\sigma_a'$ → von Mises alternating stress

$\sigma_m'$→ von Mises mean stress

$S_e$ → endurance stress

$S_{ut}$ → ultimate tensile strength

n → Factor of safety (FOS)

These alternating bending and torsional stresses are required to be calculated. These stresses are a function of the diameter of the shaft and as such, we can utilize this to size the shaft diameter under fatigue conditions. Firstly, the von Mises alternating stress is calculated as follows:

$$\sigma_a' = (\sigma_a^2 + 3\tau_a^2)^{\frac{1}{2}} \quad \text{.....(11)}$$

Recall that $\sigma_a$ is the alternating bending stress and $\tau_a$ is the alternating torsional stress. Both of these physical quantities can further be calculated as follows:

$$\sigma_a = \frac{32 k_f M_a}{\pi d^3} \quad \text{..... (12)}$$

$$\tau_a = \frac{16k_{fs}T_a}{\pi d^3} \quad \text{(13)}$$

Substituting gives the formula equivalent alternating stress referred to as the von Mises alternating stress:

$$\sigma'_a = \left[\left(\frac{32k_f M_a}{\pi d^3}\right)^2 + 3\left(\frac{16k_{fs}T_a}{\pi d^3}\right)^2\right]^{\frac{1}{2}} \quad \text{(14)}$$

In like manner, the von Mises mean stress is calculated as follows:

$$\sigma'_m = (\sigma_m^2 + 3\tau_m^2)^{\frac{1}{2}} \quad \text{(15)}$$

Recall that $\sigma_m$ is the alternating bending stress and $\tau_m$ is the alternating torsional stress. Both of these physical quantities can further be calculated as follows:

$$\sigma_m = \frac{32k_f M_m}{\pi d^3} \quad \text{(16)}$$

$$\tau_m = \frac{16k_{fs}T_m}{\pi d^3} \quad \text{(17)}$$

Substituting gives the formula equivalent alternating stress referred to as the von Mises mean stress:

$$\sigma'_m = \left[\left(\frac{32k_f M_m}{\pi d^3}\right)^2 + 3\left(\frac{16k_{fs}T_m}{\pi d^3}\right)^2\right]^{\frac{1}{2}} \quad \text{(18)}$$

Where: $k_f \rightarrow$ fatigue stress concentration factor for bending
$k_{fs} \rightarrow$ fatigue stress concentration factor for torsion
$M_a \rightarrow$ alternating bending moment
$T_a \rightarrow$ alternating torque
$M_m \rightarrow$ mean moment
$T_m \rightarrow$ mean torque
d $\rightarrow$ diameter of shaft

It is important to note that preliminary designs assumed a uniform shaft with a constant cross-sectional area. That is, the stress concentration factors will not affect the overall sizing. Reiteratively, stress concentration factors occur in materials and structures where there is a geometric irregularity, such as a notch, hole, or sudden change in shape, that causes an abrupt change in stress concentrations. In other words, $k_f = k_{fs} = 1$. The point of this preliminary design of the shaft is to identify a starting diameter that should not be compromised in order to safely transfer power from the engine to the eddy current brake.

Equations were then substituted to get the following:

$$\frac{\left[\left(\frac{32k_f M_a}{\pi d^3}\right)^2 + 3\left(\frac{16k_{fs}T_a}{\pi d^3}\right)^2\right]^{\frac{1}{2}}}{S_e} + \frac{\left[\left(\frac{32k_f M_m}{\pi d^3}\right)^2 + 3\left(\frac{16k_{fs}T_m}{\pi d^3}\right)^2\right]^{\frac{1}{2}}}{S_{ut}} = \frac{1}{n} \quad \text{(19)}$$

This formula was integrated into a MATLAB code as shown below. This was to aid in efficient calculation by eliminating as much human error as possible.

*MATLAB code:*

```
clc
clear
close all
```

```
% INPUT PARAMETERS
l = 0.1778;           % Length of the shaft (m)
E = 206e9;            % Young's modulus (Pa)
density = 7861;       % Material density (kg/m^3)
g = 9.81;             % Density of 1045 steel in N/kg
K_f = 1;              % Fatigue stress Coefficient factor for bending
K_fs = 1;             % Fatigue stress Coefficient factor for torsion
T_min = 0;            % Minimum torque in Newton-meters (Nm)
T_max = 65;           % Maximum torque in Newton-meters (Nm)
S_e = 600e6;          % Endurance Strength
S_ut = 565e6;         % Ultimate Tensile Strength

% Initial diameter guess for shaft
d = 1;

% Convergence criteria
target_FOS = 1.5;
tolerance = 1e-06;
max_iterations = 10;
for iter = 1:max_iterations
  x = 0:0.01:0.4572;
  V_shear = ((density*pi*d.^2*g)/4)*((l/2)-x);
  M_bending = ((density*pi*d.^2*g)/4)*(6*l*x - l.^2 - 6*x.^2);

  % Define bending moment function
  fun = @(x) ((density*pi*d.^2*g)/4)*(6*l*x - l.^2 - 6*x.^2);

  % Find the minimum moment using fminbnd
  [x_min_val, M_min] = fminbnd(@(x) fun(x), 0, l);

  % Find the maximum moment using fminsearch
  x_max_val = fminsearch(@(x) -fun(x), 0);
  M_max = fun(x_max_val);

  % Update FOS
  M_a = (M_max - M_min)/2 ;
  M_m = (M_max + M_min)/2 ;
  T_a = (T_max - T_min)/2 ;
  T_m = (T_max + T_min)/2 ;

  % Calculate A and B
  A = sqrt(4*(K_f*M_a)^2 + 3*(K_fs*T_a)^2);
  B = sqrt(4*(K_f*M_m)^2 + 3*(K_fs*T_m)^2);

  % Calculate FOS
```

```
    FOS = (pi*d^3/16)*((A/S_e) + (B/S_ut))^-1;

    % Display the results
    % disp(['Iteration ', num2str(iter)]);
    disp(['Diameter = ', num2str(d)]);
    % disp(['Factor of Safety = ', num2str(FOS)]);

    % Check for convergence
    if abs(FOS - target_FOS) < tolerance
        disp('Converged to the target Factor of Safety.');
        break;
    else
        % Update diameter for the next iteration
        d = d * ((target_FOS/FOS)^(1/3));
    end
end
if iter == max_iterations
    disp('Maximum number of iterations reached without convergence.')
end
d_inches = d * 39.3701;
figure(1)
plot(x,V_shear)
xlabel('Distance (m)')
ylabel('Shear Force (N)')
title('Graph showing Shear Force as a function of distance')
grid on

figure(2)
plot(x,M_bending)
xlabel('Distance (m)')
ylabel('Bending Moment')
title('Graph showing Bending Moment as a function of distance')
grid on

fprintf('Required shaft radius under fatigue conditions: %.4f inches\n', d_inches);
```

```
Diameter = 1
Diameter = 0.036708
Diameter = 0.011395
Diameter = 0.011391
Converged to the target Factor of Safety.
Required shaft radius under fatigue conditions: 0.4484 inches
>>
```

*Figure 10: Results illustration of MATLAB code*

The MATLAB script provided initially incorporates constant parameters associated with the shaft and some known applied loads. To generate the bending moment diagram, an initial estimate of the required diameter was essential. Critical points, namely the maximum bending moment ($M_{max}$) and minimum bending moment ($M_{min}$), were identified from this diagram. These values were then utilized to derive both the alternating and mean moments, serving as inputs for the modified Goodman relation in equation 19. In like manner, the torque values were determined from the specifications of the 2001 Honda CBR600 f4i engine. The maximum torque, $T_{max}$ = 65 Nm and the minimum torque, $T_{min}$ = 0 Nm. These values also served as inputs for equation 19.

The resulting output was the factor of safety (FOS). From an ethical standpoint, it is imperative for the factor of safety to be at least 1.5. Therefore, the minimum diameter necessary to achieve this factor of safety was determined. In case the factor of safety fell below 1.5, a while loop was implemented to iteratively recalculate until convergence to 1.5 or until a maximum of 100 iterations was reached. The imposition of a maximum iteration limit ensures the code's efficiency and prevents it from running indefinitely.

The computed diameter was then converted to inches, and shear and bending moment diagrams were plotted. Executing the MATLAB code revealed that the smallest feasible diameter to ensure a factor of safety of 1.5 under fatigue conditions is 0.4484 inches. This implies that any 1045 chrome-plated steel shaft should not have a diameter below 0.4484 inches. It is crucial to emphasize that these calculations served to provide an approximate value for the team to target. Subsequently, simulations were conducted on SOLIDWORKS to further validate the accuracy of the shaft design.

From the minimum diameter determined as 0.4484 inches, a generic beam representation of the shaft was illustrated in Figure 11 below:

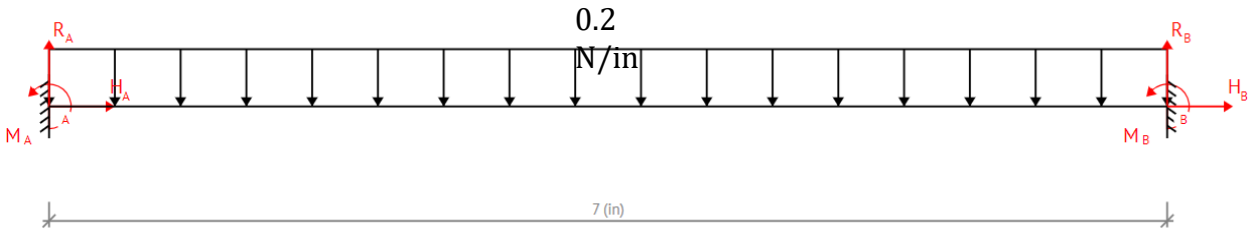


*Figure 11: Load distribution of shaft with diameter of 0.4485 in and length 7 inches*

Figure 11 depicts the uniform load distribution on the shaft when employing the recently determined diameter under fatigue conditions. This was achieved by integrating the corresponding values into equation 20:

$$w = \frac{\rho \pi d^2 g}{4} \quad \text{..... (20)}$$

$$w = \frac{(7861)\pi(0.01139)^2(9.8)}{4}$$

$$w = 7.856\ N/m$$

A shear diagram was generated on MATLAB for the specified shaft diameter, as depicted in figure 12.

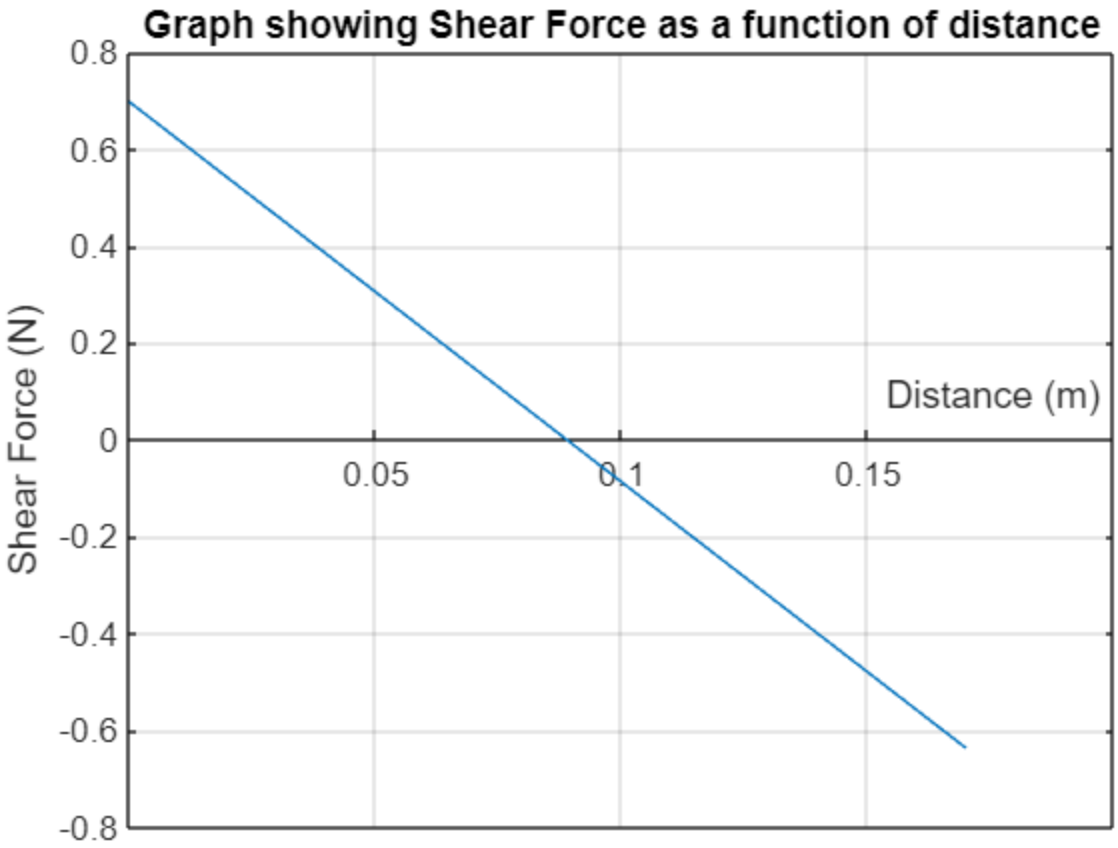


*Figure 12: Graph showing shear force as a function of distance*

Figure 12 illustrates a profile showcasing the fluctuation in shear force along the shaft. It is crucial to emphasize that the maximum shear force occurs at the shaft's ends, with opposing shear directions. It should be noted from the graph the maximum and minimum shear force experienced along the shaft. $V_{shear,min} = -0.6373\ N$ while $V_{shear,max} = 0.6986\ N$

The general formula that governed the trajectory of the graph in Figure 12 is:

$$V(x) = \omega\left(\frac{l}{2} - x\right) \quad \text{..... (21)}$$

Given that the load is a uniformly distributed load, the above formula can be rewritten as follows

$$V(x) = \frac{W}{l}\left(\frac{l}{2} - x\right)$$

The equation can further be revised given that Weight, W, is a function of the diameter hence,

$$V(x) = \frac{\frac{\rho\pi d^2 g l}{4}}{l}\left(\frac{l}{2} - x\right)$$

Simplifying the above gives the final equation below as

$$V(x) = \frac{\rho\pi d^2 g}{4}\left(\frac{l}{2} - x\right) \quad \text{..... (22)}$$

A bending moment diagram was generated on MATLAB for the specified shaft diameter, as depicted in figure 13.

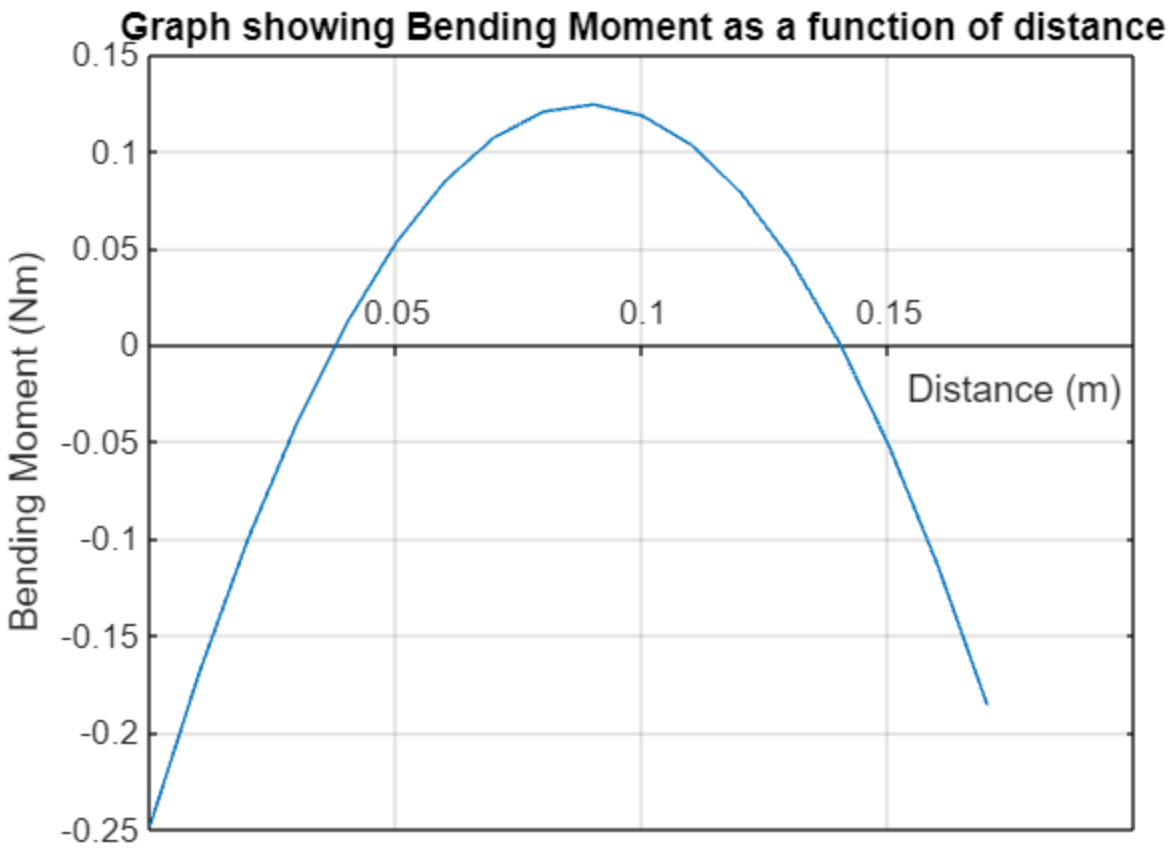


*Figure 13: Graph showing bending moment as a function of distance*

Figure 13 illustrates a profile showcasing the fluctuation in bending moment along the shaft. It is crucial to emphasize that the maximum bending moment occurs at the center of the shaft.

The general formula that governed the trajectory of the graph in Figure 13 is:

$$M(x) = \frac{\omega}{12}(6lx - l^2 - 6x^2) \quad \text{..... (23)}$$

Given that the load is a uniformly distributed load, the above formula can be rewritten as follows

$$M(x) = \frac{\frac{W}{l}}{12}(6lx - l^2 - 6x^2)$$

The equation can further be revised given that Weight, W, is a function of the diameter hence,

$$M(x) = \frac{\frac{\rho\pi d^2 gl}{4}}{12l}(6lx - l^2 - 6x^2)$$

Simplifying the above gives the final equation below as

$$M(x) = \frac{\rho\pi d^2 g}{48}(6lx - l^2 - 6x^2) \quad \text{..... (24)}$$

**3.1.3 – Dynamic Conditions**:

The critical speed of a shaft is the rotational speed at which the shaft experiences resonance, leading to significant vibrations and potentially catastrophic failure. It is a crucial parameter in mechanical engineering, especially in rotating machinery such as motors, turbines, and pumps.

The shaft exhibits instability at specific velocities, causing deflections to escalate indefinitely. Fortunately, even in the absence of knowledge regarding the dynamic deflection shape, employing a static deflection curve provides a reliable approximation of the lowest critical speed. This curve satisfies the boundary condition of the differential equation (zero moment and deflection at both bearings), and the precise shape of the deflection curve does not significantly impact the shaft's energy. Engineers should aim to design for critical speeds that are at least twice the operational speed. Ensuring that the critical speed is at least twice the operational speed is standard practice in engineering in order so that resonance and its associated negative effects can be avoided. The formula governing the shaft's critical speed is expressed by equation

$$\omega = \left(\frac{\pi}{l}\right)^2 \sqrt{\frac{EI}{M}} \quad \text{..... (25)}$$

Where: M → mass per unit length in kilograms per meter (kg/m)

$\omega$ → speed of shaft in radians per second (rad/s)

For our purposes with the shaft, the formula can be modified to

$$d = \sqrt{\frac{16\rho}{El}} \cdot \omega \cdot \left(\frac{l}{\pi}\right)^2 \quad \text{..... (26)}$$

The maximum speed of the engine will be 6000 rpm due to the restrictor. This engine speed needed to be correlated to the output speed applied onto the shaft. This was determined using the gear ratio formula. For the 2002 Honda cbr600 f4i engine at present, the gear ratio at 6$^{th}$ gear is 1.075. 6$^{th}$ gear was chosen because maximum speed happens at the highest gears. By utilizing the gear ratio equation below, the output RPM onto the shaft was determined as follows:

$$Output\ RPM = \frac{Input\ RPM}{Gear\ Ratio} \quad \text{..... (27)}$$

$$Output\ RPM = \frac{6000\ RPM}{1.075}$$

$$Output\ RPM = 5581\ RPM$$

The above output RPM is the speed subjected to the shaft by the engine. It is now required to convert this output speed to radians per second. This is done as follows:

$$Angular\ speed = output\ RPM \times \frac{2\pi}{60} \quad \text{..... (28)}$$

$$Angular\ speed = 5581 \times \frac{2\pi}{60}$$

$$Angular\ speed = 585\ rad/s$$

For the sake of a safe design, that critical speed was doubled so the input $\omega = 2 \times 585\ rad/s = 1170\ rad/s$

This critical speed is then

$$d = \sqrt{\frac{16 \cdot (7861)}{(206 \times 10^9)(0.1778)}} \cdot (1170) \left[\frac{(0.1778)}{\pi}\right]^2$$

$$d = 0.006944\ m$$

It is standard practice to source shaft diameter sizes in the US on the imperial scale hence this diameter was then converted to inches as follows:

$$d = 0.006944\,m \times 39.3701\,\frac{in}{m}$$
$$d = 0.27\,in$$

Now, this diameter accommodates the rotational speed but does not take into consideration the torque being applied to the shaft. In order to fully validate this value, another formula needs to be integrated into the analysis. This formula is sometimes referred to as the torsion formula and it is shown in equation below

$\tau = \frac{Tc}{J}$ …… (29)

Where: $\tau \rightarrow$ Shear stress in Pascals (Pa)

T → Torque in Newton-meters (Nm)

c → maximum radius of shaft in meters (m)

J → polar moment of inertia in $m^4$

$J = \frac{\pi}{2}c^4$ …… (30)

The polar moment of inertia was first determined as follows:

$$c = \frac{d}{2} = \frac{0.006944\,m}{2} = 0.003472\,m$$

This is now used in order to find the polar moment of inertia, J,

$$J = \frac{\pi}{2}c^4$$
$$J = \frac{\pi}{2}(0.003472\,)^4$$
$$J = 2.283 \times 10^{-10}\,m^4$$

The value of J, now incorporated, was further used to find the shear stress. In the following equation, the torque, T, is identified as 65 Nm according to the engine specifications. The shear stress calculation is as follows:

$$\tau = \frac{Tc}{J}$$
$$\tau = \frac{(65)(0.003472)}{(2.283 \times 10^{-10}\,)}$$
$$\tau = 989\,MPa = 0.989\,GPa$$

Comparing this with the maximum shear stress for 1045 chrome-plated steel, which is 80.0 GPa, a ratio can be calculated to quantify the magnitude of 'Twist Safety'.

$Twist\ Safety\ = \frac{Maximum\ material\ shear\ stress}{Actual\ Shear\ Stress} = \frac{80.0\ GPa}{0.989\ GPa} = 81$ ……..… (31)

With a value of 81, this indicates that the shear stress endured by the shaft under a torque of 65 Nm is more than 80 times lower than the material's shear strength. This additional confirmation reinforces the safety of the chosen diameter for dynamic conditions under a specified torque.

For operational safety, a required shaft diameter of 0.27 inches is stipulated, considering the potential for unforeseen deflections. These unanticipated deflections could result in shaft failure, culminating in a break. Additionally, it was anticipated that the maximum shaft diameter would be tailored to dynamic conditions, given that dynamic conditions entail increased loads due to external forces and torques.

Upon thorough analysis of the shaft under various conditions, the dynamic analysis revealed the maximum shaft diameter. As previously hypothesized, dynamic conditions impose more substantial loads, making the identification of the maximum shaft size particularly relevant in this context. The conclusion drawn from this comprehensive examination is that the optimal shaft diameter, meeting all specified criteria for safe operation, should be a minimum of 0.27 inches. This determination underscores the importance of considering dynamic factors in the design process, ensuring that the chosen dimensions can effectively withstand the varying and often more demanding conditions encountered during operation. By prioritizing safety in the selection of the shaft diameter, engineers aim to guarantee the reliability and durability of the system under diverse operational scenarios, providing a robust foundation for effective and secure performance.

### 3.2 Frame

The frame was designed by the previous senior design group, who started this project. The base was already welded together, along with the base plate. The base section is made up of 2 in x 2 in square tubing, 0.065 inches thick. The base plate's dimensions are 22(l) x 18(w) x 0.25(h) inches, welded to the frame with an offset of 1 inch from the left edge of the frame (from top view). The base plate is made up of 4130 Alloy steel. The strength and weldability of this type of steel are ideal for this project's application.

Performing an FEA on the frame with five fixed areas, representing the placement of five wheels, and three hundred-pound (300lb) loads on the pillow block stands to simulate the weight of the Eddy Brake, the maximum von Mises stresses determined were 18.528 MPa, which is quite small compared to the yield strength of the material, which is 325 MPa. The Factor of Safety determined was 17.541, which is significantly higher than the industry standard of 1.5. Based on the results from the FEA, the base section of the frame is viable for the project. Between the two 60-inch metal tubing, in the area where the engine is placed, there are two smaller rectangular areas made of 1.5 x 1.5 x 0.065 in. These sections are added to the frame to accommodate two rear engine mounts, not only used to distribute the weight of the engine but also to add stability and reduce the vibration of the engine. The cabinet section of the assembly is built with 1 x 1 x 0.12 in square tubing. It rises 38 in upwards from the base of the frame. It is 23 in long and 38in wide, with two levels for shelves apart from the base frame section.

The base for these shelves is made of ¾ in ply board. The lowest level (on the base frame) will house the fuel tank. The gear shifter base is also mounted on this level. The second(middle) shelf is split into two sections. It will hold the four batteries used to power up the Eddy Brake. The second level holds the battery which will be used to provide power to the engine, the fuse and relay box, and the power modulator and Arduino. The base will hold the four batteries used to power up the Eddy Brake. The back section houses other electrical components such as the inverter and fuse box. The front section houses the fuel tank. The top shelf is delegated to hold the device used to manipulate power, extra screens, and any other items required to operate the unit. A master switch, an emergency shutoff switch, and a start button are fixed onto the front left corner of the top shelf. A throttle trigger is fixed onto the right front corner of the top shelf.

*Figure 14: Complete Frame built (left view)*

Figure 14 above shows pictures of the completed frame with five wheels installed. The top left section will be fitted with boards to form cabinets. When the boards are fastened, electrical components will be placed in the cabinets. The right section will be fitted with the engine, Telma retarder (Eddy current Brake), Engine Mounts, Pillow Block Bearings and Stands and coupling mechanisms.

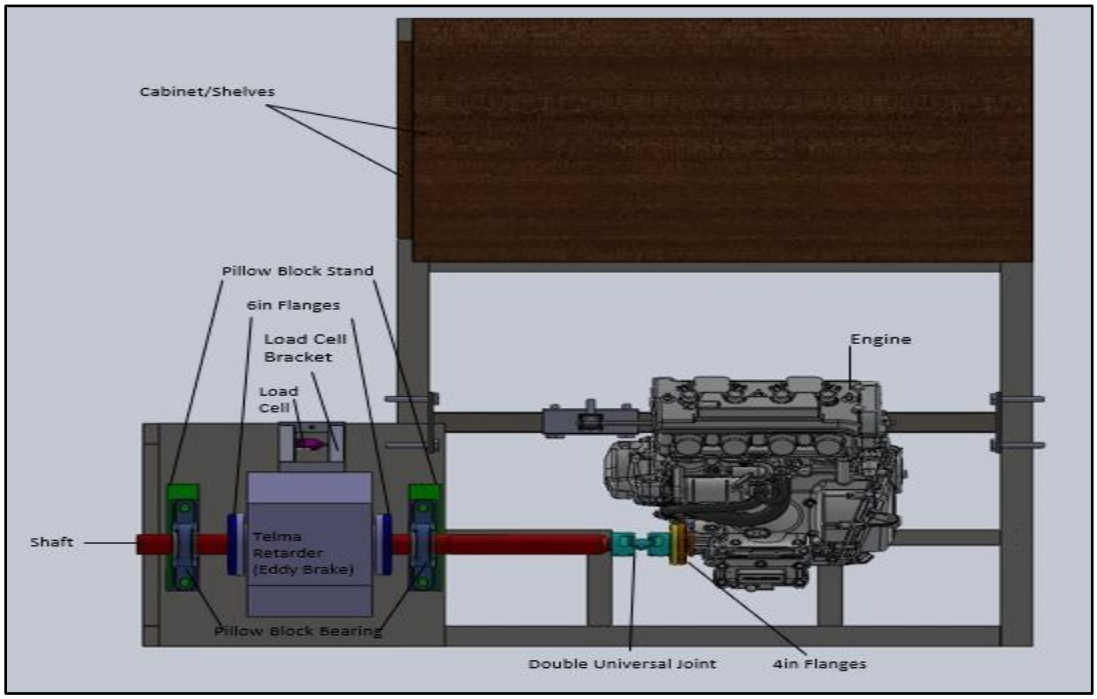


*Figure 15: Top View of Engine Dynamometer Assembly with components previously described in different colors*

The figure above is a top view of the "engine dyno" assembly with components focused on by this group so far, highlighted in different colors. Colors are as follows:

### 3.3 Components of the power transmission:

#### 3.3.1 Flanges

Flanges are components commonly used in engineering as a coupling mechanism [20]. A flange is a circular-shaped object, projecting like a cylinder, capable of being fastened onto another component, translating the same motion as that component. For this project, flanges are used to connect shafts, a double universal joint, and a sprocket within the assembly. A total of four flanges are used in the assembly: two 6in diameter and two 4in diameter. Initially, a choice had to be made between using flanges or collars. The group discussed the pros and cons of each, considering the overall design of the assembly. Collars can work but they would have to be welded to flanges on the Eddy Brake side. The Eddy Brake already had four mounting holes and a circular surface(flange) for mounting. It is more practical machine coupling flanges to match, then to weld the machined flanges to shafts, as it is not likely that these joints would need to be disassembled. On the engine side, flanges were selected instead of collars due to several considerations [21, 22].

The Double Universal Joint [23] needed to be coupled with the sprocket, and the sprocket had to be changeable, fitting any other engine to be tested. It was more feasible to weld a flange to one side of the double universal joint, then use a coupling flange to attach the sprocket. The coupling flange and the sprocket are welded together. A collar would not be ideal for this section as the diameters of the universal joint and the sprocket has significant differences. The material used to create these flanges were high-strength 1045 Carbon Steel, 0.5 in long. It has a listed yield strength of 530 MPa. The engine side of the 4in flange on shaft assembly was machined with four threaded ¼ -20in holes to facilitate quicker and easier assembly.

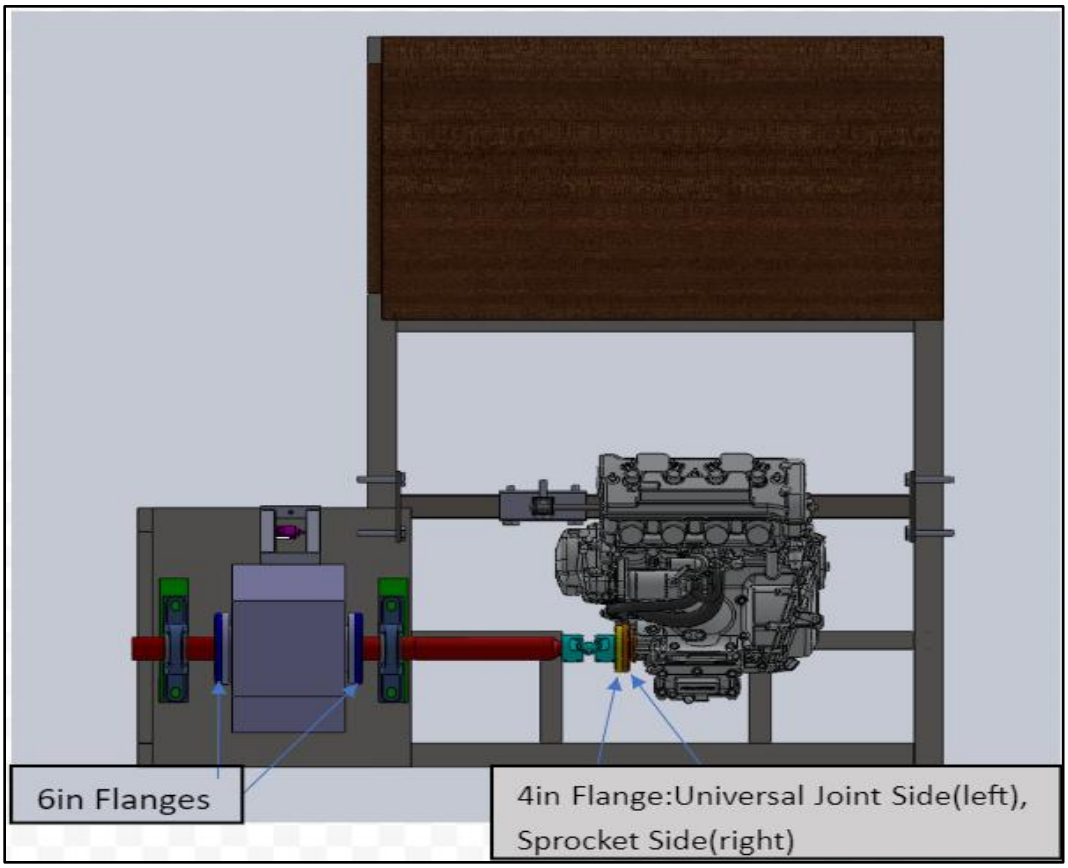


*Figure 16: Engine Dynamometer SolidWorks drawing highlighting the Flanges*

Above, a top view of the Assembly Drawing is shown with arrows indicating where the Flanges are used. Colors are used to highlight the components.

A total of four flanges are used in this assembly. Two similarly designed 6-inch flanges are used, one on each side of the Eddy Brake. On the back side of the Eddy Brake, the flange is used to connect the Eddy Brake to a Pillow Block Bearing. On the front side (engine side), the flange is used to connect the Eddy Brake to the engine through another Pillow Block Bearing. On the "engine side" of the assembly, two 4-inch flanges with different designs are used. They are connected to each other eventually. One flange has a "through cut" with a diameter of 1.54 inches. This cut is incorporated into the design to allow the partial insertion of a sprocket, which will be welded onto the flange. When the sprocket is welded to this flange, a fastening bolt and washer will be used to fix this flange onto the transmission output shaft, restricting lateral movement in this section. The depth of the flange is enough for the fastening bolts to sit between the transmission output shaft and the coupling flange. Deciding to weld the sprocket instead of machining internal gears was an easy choice.

Machining internal gears requires much more time and resources compared to purchasing a sprocket with the internal gear already built in. This flange has four symmetrical holes, distanced 1.6inches from the center of the flange, with internal 5/16-18 threads, to allow attachment of the other flange via 5/16-18 bolts. Internal threads were selected instead of nuts due to the limited space available behind the sprocket, which would make assembling more difficult. The other 4in flange connecting to the double universal joint on the shaft side, is machined with four symmetrical holes with 5/16in diameter to accommodate bolts. These holes are bare as the design requires threads only on the 4-inch coupling flange. The holes were spaced 1.6 inches away from the center

of the flange. This distance was determined by measuring features on the coupling flange. On the front side of this flange, a 1.6 in diameter through cut will be made. This through cut is to assist with the alignment of the connecting universal joint, and to allow more surface areas to weld. With the through cut, welding can be done on the face closer to the body of the universal joint, also on the inside of the through cut. Performing an FEA on the flanges confirmed the spacing and distance decision.

All flanges have their front edges chamfered to reduce the chance of injury when handling.

### 3.3.2 - Double Universal Joint

A universal joint is a connecting mechanism that allows the transmission of torque from one component to another, even while the components rotate about different axes. For this project, a HUCO Double Universal Joint 63175800 was used to connect the drive shaft to the engine. A double universal joint was chosen as alignment needed to be compensated for both vertically and horizontally. The component consists of two single universal joints connected in tandem with a center section, allowing angular misalignment compensation greater than that of a single universal joint. Its design is precision-engineered, transferring smooth and efficient torque transmission. This universal joint is capable of handling torques of up to 171.6 Nm, ideal for this assembly, which produces 65 Nm at its maximum. Its strength is credited to the high-quality steel it is built with. The maximum operating angle permitted by this design is 90°, ideal for this project.

Using a double universal joint reduces the number of connection points or points that need welding from four to two. Using two individual universal joints would have required two welded sections on each joint, a total of four welds to the assembly. One end of the double universal joint will be connected to the shaft, while the other end will be welded to the 4-inch flange. The outer diameter is 2.283 inches, while the inner diameter (bore) is 1.18 inches. Such sizing is ideal and complements the rest of the assembly as the minimum calculated shaft diameter size is 1.13 in, and the outer diameter of the shaft is 1.935 inches. The bore contains a keyway, which will allow ease when connecting. The keyway is ideal for both alignment and torque transmission. In terms of length, the total length is 7.165 inches when fully extended along the same plane.

*Figure 17: Photo of HUCO Double Universal Joint [23]*

Figure 17 above shows a photo of the Double Universal Joint sold by HUCO. This device is used in the assembly to compensate for misalignment and to transfer torque from the shaft to the Eddy Brake.

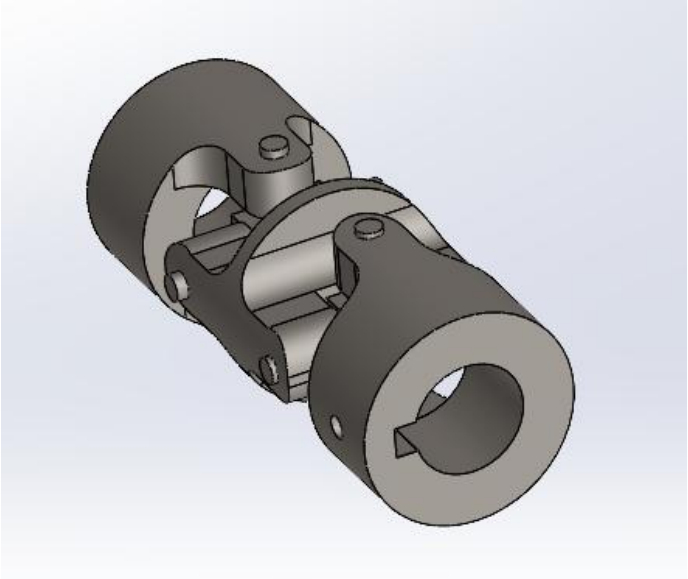

*Figure 18: CAD picture of double universal joint*

### 3.3.3 - Pillow Block Stands

Welded to the base plate on the frame, the Pillow Block Stands are metal U-shaped stands designed to hold the Pillow Block Bearing at a particular height above the Base Plate. This height will allow the Eddy Brake to be suspended above the Base plate and will permit rotation within set limits. Based on the Pillow Block Bearings obtained from McCoy College of Science, Mathematics and Engineering, with a dimension of 10.5 in long and 2.5 in wide, the Pillow Block Stands are built with 2 x 2 x 0.065 in metal tubes. They stand 5.75 in tall and are 10.5 in long. Three pieces of tubing are welded, with the ends of the top tubing section open to allow the installation of a bolt to a washer and nut on the inside of the tube. This bolt is used to fasten the Pillow Block to the Pillow Block Stand.

### 3.3.4 Pillow Block Bearings

Pillow Block bearings are bearings situated inside of a robust metal structure. A pillow block bearing is a type of mounted bearing unit designed to provide support and facilitate smooth rotational motion for a shaft. It consists of a housing, often resembling a pillow or block shape, with a bearing installed inside. The bearing typically contains an inner and outer ring, balls or rollers, and a cage to maintain separation and proper alignment of the rolling elements. This assembly is mounted onto a surface and secures a rotating shaft within the housing, allowing it to move freely while providing support and reducing friction. In this case, the metal structure is made of cast iron. The bearing should be able to withstand loads of at least 300 lbs. statically, as this is the approximate weight of the components supported by the bearings are approximately 250lb. The maximum revolutions per minute of the engine output shaft is 6000 RPM. This value is the limit set by FSAE. Considering the gear ratio in 6th gear, which will output the highest revolutions per minute, the output shaft of the transmission will deliver 5309.73RPM. The bearings, therefore, must be rated for operating at higher RPMs than this for safe use. Shaft collars are used with these bearings to prevent horizontal movement of the shafts.

*Figure 19: SealMaster Pillow Block Bearing*

Figure 19 above shows a picture of a SealMaster Pillow Block Bearing, with the style and design expected to be implemented into the assembly (Figure 20).

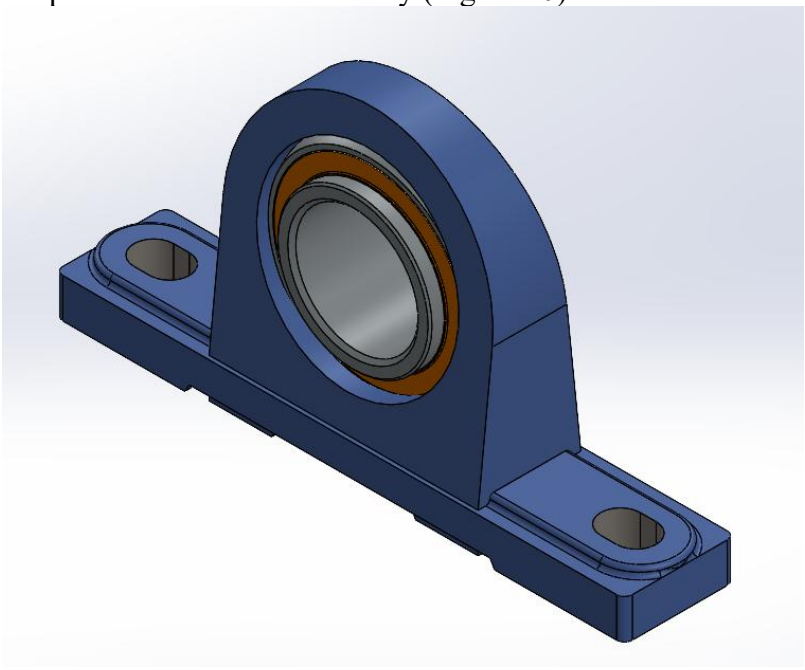

*Figure 20: CAD picture of Pillow block bearing*

### 3.3.5 Load Cell Bracket

The Load Cell Bracket is a component that attaches the Load Cell to the Eddy Brake. On the side of the Eddy Brake, there are three threaded holes in which a bracket is usually mounted to hold the Eddy Brake in place. In the Engine Dyno setup, there is no need for the Eddy Brake to be mounted using brackets, as the Eddy Brakes need to rotate within specific limits. The Eddy Brake is mounted on the Pillow blocks. The holes in the Eddy Brake's frame are now used to fasten the Load Cell Bracket. The Load Cell Bracket is made up of 1 x 1 x 0.12 in metal tubing, made from 1010-1026 Low Grade Carbon Steel.

### 3.3.6 - Engine Rear Mount

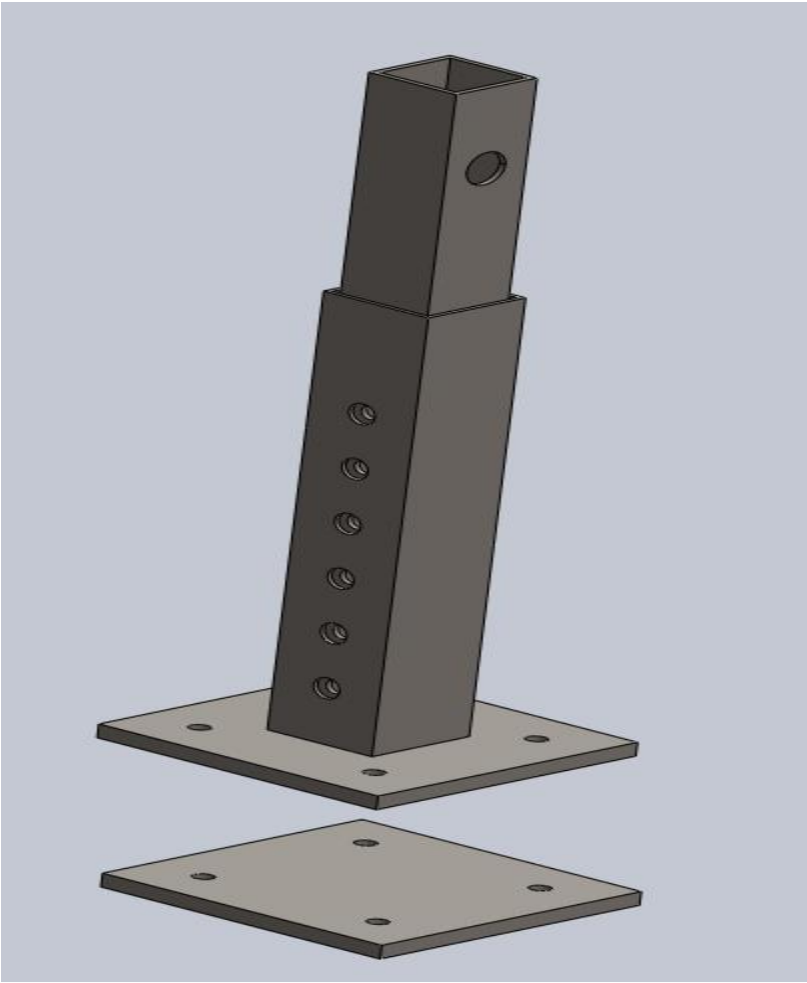

*Figure 21: Rear mount with bottom mounting plate*

The rear mounts take on a similar design to the front mounts. It is a combination of three parts: a base, inner tubing, and outer tubing. The base is made with 0.25in thick 1018 steel, cut into two $4\ in \times 4\ in$ plates. Four 0.25in holes are drilled into the plate in a square pattern, with a 1.5 in spacing. The outer tube is made with 1.25 in square tubing, 0.063 in thick. It is welded in the center of the base, leaving 1.25 in on each side. The inner tube is made with 1in square tubing. Holes which are 0.25 in are machined into both tubes at 1in spacing, through parallel sides. Through the two other faces of the inner tube, a 0.75 hole is machined to accommodate a steel rod of similar diameter, which passes through both rear mounts and the engine. This steel rod supports the weight of the engine. The rear mount is fixed onto the frame using a coupling base plate. The coupling base plate has the same dimensions and machined properties as the original base plate.

The buckling analysis deals with predicting the critical loads at which a structure would likely undergo buckling. Buckling is a sudden and catastrophic mode of failure. This particular part was the basis of our study for the rear mount, as it has the largest surface area on which the load is applied, while the overall area of the metal tubing is the smallest. The outer tube would be able to withstand higher loads as it has a larger surface area. Also, the inner tube is slender and longer than the outer tube. The mathematical formula for buckling, developed by Euler, is given by

$$P_{cr} = \frac{\pi^2 E I}{(K L)^2} \quad \text{.....(32)}$$

Where:
$P_{cr}$ is the critical buckling load(the load at which buckling occurs),
E is the modulus of elasticity of the material,
I is the moment of inertia of the column's cross-sectional area,
K is the column's effective length factor(depends on the end conditions of the column),
L is the length of the column.
From this formula, we see that the length of the column directly relates to the critical buckling load.

### 3.3.7 Radiator Mount

Welded onto the left side of the middle level are two metal tabs. They are 1.5in * 3in rectangles with a 3/16in hole drilled into it at 0.75in from the short edge. These tabs are used to mount the "stock radiator," which was initially mounted on a motorcycle with the engine that is currently used for testing.

### 3.3.8 Gear Shifter

The gear shifter allows transitioning between the gears. It consists of three main components: A base that allows pivot, a lever, and a connecting rod. The lever is made with metal tubing, 1in diameter, 0.049in wall thickness, extending 42in long. On the top section, a handle is fixed in place. On the handle is a trigger, used to engage and disengage the clutch. The connecting rod is made of the same metal tubing as the gear shifter lever, and is 40in long. Both ends are fitted with 4in long rods, with 3/8-20 threads. The threaded regions allow adjustment for shifting. One end is fastened to the gearshift lever's adapter using two nuts and lock washers. The other end screws into an adapter that connects to the transmission. They also allow fastening in place via two nuts on one end.

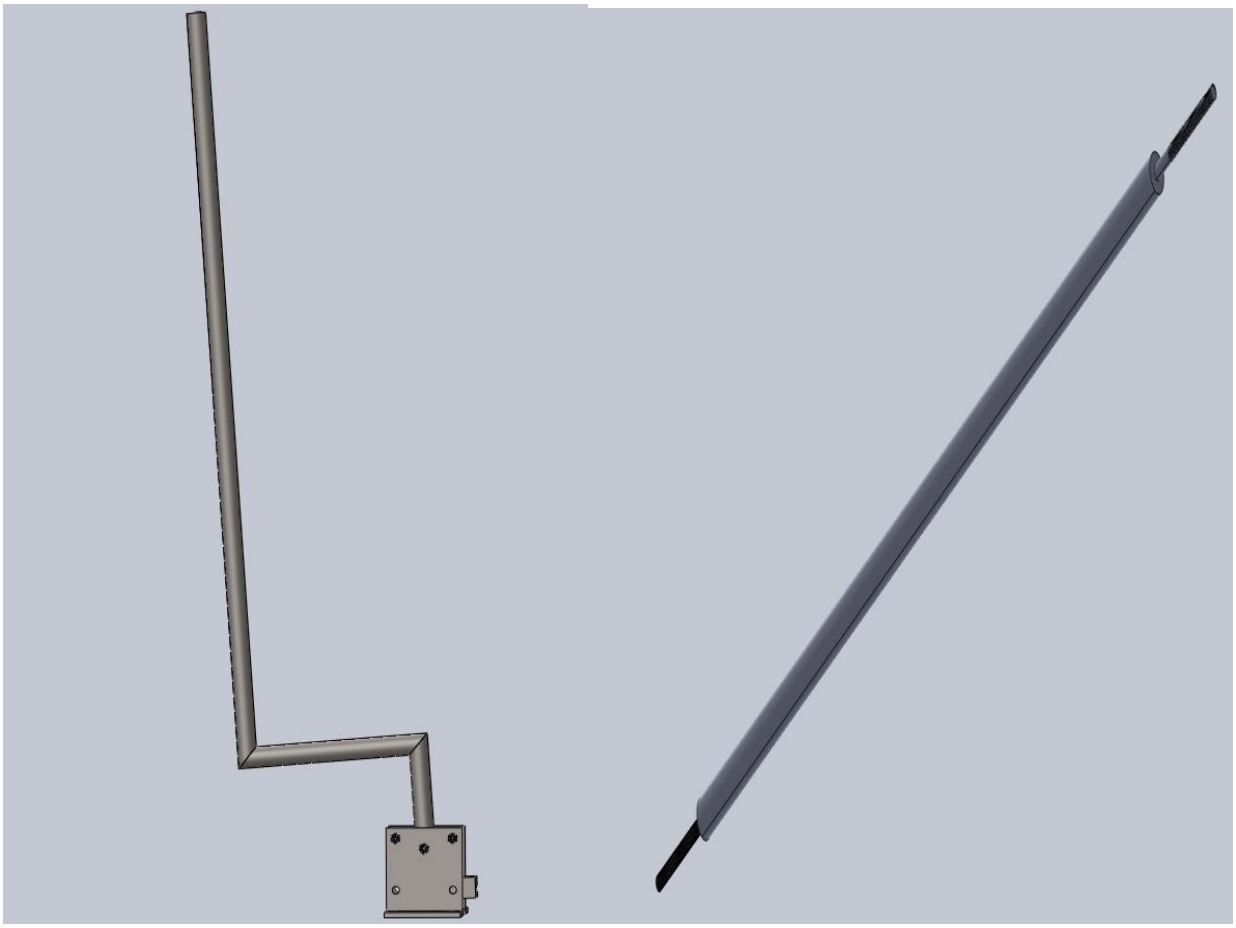

*Figure 22: 3D model of Gear Shifter Lever and Base assembly (left) and Connecting Rod (right), without handle and trigger*

### 3.3.9 Generator

Initially, the engine dyno was powered by a DC power source consisting of four 12-volt batteries, as depicted in figure 23 below. The power inverters were chosen based on their working principle [24].

*Figure 23: Four 12 V DC Batteries 100 Ah*

However, this approach was abandoned in early February 2024 due to malfunctions with the 3000 Watt WZRELB inverter, shown in figure 24 below.

*Figure 24: 3000 W Inverter*

The inverter encountered problems when the Arduino transmitted a relatively high fraction of the maximum voltage to the eddy current brake. Despite inconclusive results from a root cause analysis, symptoms suggested an overload within the inverter. Despite exhaustive troubleshooting by the team, no solution was found, leading to the adoption of an alternative energy source. The availability of a DuroMax XP13000EH Dual Fuel Portable Generator, as depicted below, offered a remedy by delivering direct 240V power to the YourDyno power supply.


*Figure 25: Generator providing 240 V at 30 A to YourDyno power supply*

The adoption of this alternative solution eliminated around $1000 in project expenses. While the generator provides versatility for different setups beyond the battery inverter arrangement, it requires additional space for dyno operation and produces significant noise, which could potentially impair the operator's ability to distinguish engine-specific sounds.

### 3.3.10 YourDyno Eddy current brake power supply

Connected with the eddy current power supply after the inverter. The inverter will produce AC power, which aligns with the input requirements of the eddy brake power supply. The eddy brake power supply operates with an AC input voltage of 220 – 240 V, producing a variable DC output of 0 – 96V at a maximum current of 30 A. It accepts a 5 V Pulse Width Modulation (PWM) control input. Pulse Width Modulation (PWM) is a technique used to encode analog information in a digital signal. In PWM, the duration of a pulse within a fixed period represents the amplitude of

the analog signal being encoded. This means that the average value of the signal is varied by changing the width of the pulse while keeping the frequency constant.

*Figure 26: Eddy current power supply*

The eddy current power supply is designed to integrate either with an instrument kit available for purchase on yourdyno.com or with a microcontroller like Arduino. The previous team opted for Arduino due to its cost-effectiveness compared to the $1000 instrument kit. They noted that while online forums indicated that Arduino usage was feasible, it required custom coding. To demonstrate the braking capabilities of the eddy current brake, the team devised a code linking digital pin 9 of the Arduino to the signal port and the GND pin to the 0V port on the power supply. Subsequently, the code depicted in Figure 27 was transmitted to the Arduino, purportedly resulting in the eddy brake exerting half of its braking power, assuming that half of the PWM signal was transmitted to the power supply via Arduino.

```
const int brakePin = 9; // Pin connected to the eddy current brake
const int dutyCycle = 128; // Desired duty cycle (0 to 255)


void setup() {
  Serial.begin(9600); // Open the serial port at 9600 bps:
  pinMode(brakePin, OUTPUT); // Set the brake pin as an output

  // Set the power to the brake with constant duty cycle
  analogWrite(brakePin, dutyCycle);
}


void loop() {
  // Print the current duty cycle to serial monitor
  Serial.println(dutyCycle);

  // No delay, continues looping immediately
}
```

*Figure 27:Arduino code used to control braking force*

### 3.3.11 Parallel vs Series specifications

| Voltage | 12 V | 24 V |
|---|---|---|
| Resistance per coil | 0.49 Ω (± 5% at 20℃/ 68℉) | |
| Resistance per circuit | 0.25 Ω (±5% at 20℃/ 68℉) | 0.98 Ω (± 5% at 20℃/ 68℉) |
| Current draw per circuit | 49 A (± 5% at 20℃/ 68℉) | 24.5 A (± 5% at 20℃/ 68℉ ) |
| Insulation resistance | >1 MΩ | |
| Number of stages | 4 | |

*Figure 28: Electrical Specifications*

The strategic decision to rewire the stages in series allowed us to minimize the amperage necessary to power up the eddy brake. Incorporating calculations based on coil specifications, including total inductance, total resistance, and time constant, this ensured that our rewiring decisions were rooted in sound engineering principles. These calculations contributed to an optimized performance balance, enabling a precise and finely adjustable braking system.

### 3.3.12 AF50-90 Retarder (Series Configuration)

Connected with the output of the eddy current power supply to the AF50-90 retarder. The retarder, configured with a series arrangement of stages, each with specific voltage and current specifications, will receive the necessary electrical current to generate eddy currents and produce controlled braking forces. In this setup, the retarder operates at 24V per circuit, with a resistance of 0.98 ohms per circuit and a current draw of 24.5A. The AF50-90 retarder has a total braking power of 94 kW. Since the AF50-90 retarder was configured with a single stage, the power stages are straightforward. The eddy brake power supply outputted the required voltage (96V) and current (30 A) to power up the retarder.

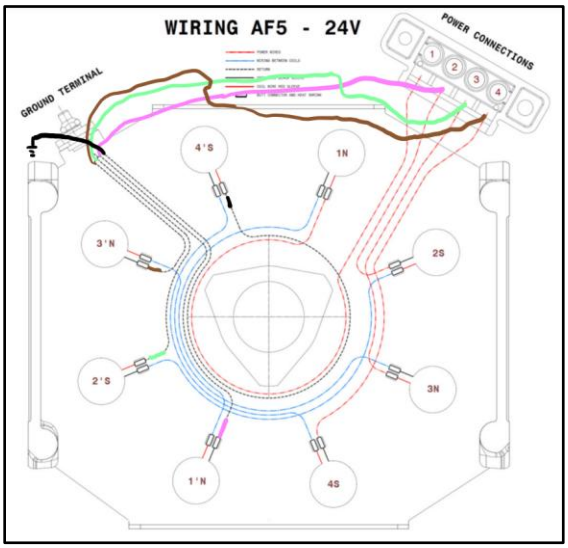


*Figure 29: Wiring configuration in series*

The configuration decision to connect each circuit in series within a stage while also arranging the stages in series revealed a strategic approach to manage the electrical demands of the AF50-90 retarder effectively. Although each circuit within a stage is in series, aligning the stages in series minimized the total current draw, providing a solution to accommodate the constraints of the eddy power supply with its 30 A maximum output. This design choice showcased a careful balance between the desired braking performance and the practical limitations of the power supply. By arranging the series connection of both circuits within a stage and stages themselves, the AF50-90 retarder optimized its operational efficiency, ensuring compatibility with the available power infrastructure while maintaining its capability to deliver precise and powerful braking forces in dynamic testing scenarios on our engine dynamometer.

Power up calculations in parallel per stage:

| **Formula** | **Results** |
|---|---|
| $Voltage = V_1 = V_2 = V_3 = V_4 = V_{total}$ | $12V_1 = 12V_2 = 12V_3 = 12V_4 = 12V$ |
| $Current = I_1 + I_2 + I_3 + I_4 = I_{total}$ | $49A_1 + 49A_2 + 49A_3 + 49A_4 = 196A$ |
| $Resistance(\frac{1}{R}) = \frac{1}{R_1} + \frac{1}{R_2} + \frac{1}{R_3} + \frac{1}{R_4} = R_{total}$ | $\frac{1}{R} = \frac{1}{.25_1} + \frac{1}{.25_2} + \frac{1}{.25_3} + \frac{1}{.25_4} = 0.0625\Omega$ |

This high current draw underscored the amps coming from the eddy power supply. This is why we took in consideration rewiring the eddy brake circuit in series and the stages in series as well.

Power up calculations in series:

| **Formula** |
|---|
| $Voltage = V_1 + V_2 + V_3 + V_4 + V_5 + V_6 + V_7 + V_8 = V_{total}$ |
| $Current = I_1 = I_2 = I_3 = I_4 = I_5 = I_6 = I_7 = I_8 = I_{total}$ |
| $Resistance = R_1 + R_2 + R_3 + R_4 + R_5 + R_6 + R_7 + R_8 = R_{total}$ |
| **Results** |
| $12V_1 + 12V_2 + 12V_3 + 12V_4 + 12V_5 + 12V_6 + 12V_7 + 12V_8 = 96V$ |
| $24.5_1 = 24.5_2 = 24.5_3 = 24.5_4 = 24.5_5 = 24.5_6 = 24.5_7 = 24.5_8 = 24.5A$ |
| $0.49_1 + 0.49_2 + 0.49_3 + 0.49_4 + 0.49_5 + 0.49_6 + 0.49_7 + 0.49_8 = 3.92\Omega$ |

This low current and voltage draw scored the amps and voltage coming from the eddy power supply. This was ideal for the performance of our Engine dyno.

This comprehensive procedure ensured a well-coordinated and efficient power supply system, facilitating precise and controlled braking forces during dynamic testing on the engine dynamometer.

The successful integration of the power supply system, eddy brake, and associated components within our engine dynamometer exemplified a meticulously planned and seamlessly executed engineering feat. The compatibility of each element has been a focal point, ensuring a harmonious interplay of systems for accurate and controlled dynamic testing scenarios.

The integration process involved a careful alignment of voltage and current specifications, from the DC power source to the AF50-90 retarder. The series configuration of the eddy brake stages, coupled with the series arrangement of coils within each stage, enhanced adaptability and responsiveness. This design choice, alongside the judicious selection of the inverter and eddy brake

power supply, optimized the power supply system's efficiency and aligns with the practical constraints of the dynamometer setup.

### 3.3.13 - Engine Control Unit (ECU)

The Engine Control Unit (ECU), alternatively referred to as the Engine Control Module (ECM) or Powertrain Control Module (PCM), stands as a vital component within modern vehicles. Acting as the central intelligence hub for the engine management system, it orchestrates a range of functions to enhance engine performance, fuel efficiency, and emissions control.

Its primary functions encompass:

- **Engine Management:** Fine-tuning fuel injection timing, air-fuel ratio, ignition timing, and idle speed across diverse driving scenarios to achieve optimal engine performance.
- **Emissions Control:** Monitoring and adjusting fuel delivery and combustion parameters to minimize harmful emissions, aligning with environmental standards.
- **Diagnostic Monitoring:** Continuously scrutinizing engine sensors to detect irregularities or faults, prompting warning signals and storing diagnostic codes for diagnostic purposes.
- **Adaptive Control:** Employing adaptive algorithms to adjust engine parameters dynamically based on sensor feedback and driving conditions, refining performance and efficiency over time.
- **Integration of Safety Features:** Serving as a communication hub between the engine and other vehicle systems, including transmission, brakes, and stability control, to synchronize operations and bolster vehicle safety.

Our chosen ECU is the Performance PE3-3400 waterproof model, selected for its unique ability to handle Cylinder 4 stroke engines without the need for additional external igniters. Moreover, it efficiently manages the unsaturated/high impedance injectors of the CBRf4i in a sequential firing sequence. Accessible via performance electronics software on a laptop, this ECU facilitates seamless operation. Furthermore, it integrates with other microprocessors through CAN BUS communication, making it an indispensable component of the Dynamometer's Data Acquisition (DAQ) system. Its role includes transmitting engine data gathered from sensors and other engine components.


*Figure 30: PE3 performance electronics ECU*

This ECU is quite versatile and has many specifications that meet the needs of any engine tuning as it relates to optimizing the performance of the engine. The general system features include:

- PC Based Tuning Software,
- Ethernet Connectivity (Wi-Fi Capable), Waterproof Enclosure
- Pulse-2-Sync™ MAP Sensor Cam Sync
- Drive-2-Tune™ Technology
- Dedicated CAN Bus
- Up to 20 Hours of Data Logging
- Extensive Failsafe Functions
- Map Switching
- 1 to 8 Cylinders
- 2 or 4 Stroke

The fuel and injection specific control include:

- Individual Cylinder Trims
- Dual Sensor Closed Loop O2 Control with Adaptive Learning
- Sequential, Semi-Sequential or Staged Injector Firing
- 8 Saturated or Peak-and-Hold Injector Drivers
- Coil-On-Plug, Wasted Spark or Distributor Ignition
- 4 Coil Drivers with Built-In Igniters

The system inputs and outputs include:

- 6 Dedicated Inputs (Crank, Cam, IAT, ECT, MAP, TPS)
- 8 Analog Sensor Inputs (0-5 Volt) – Up to 2 Temperature Inputs
- 7 Switched Inputs – Up to 4 Frequency Inputs
- 10 Configurable On/Off Outputs – 8 PWM Outputs
- Dedicated Tachometer Driver
- Idle Air Control

## 4 Results:

### 4.1 Finite Element Analysis of the design (all aspects relating to shaft design)

#### 4.1.1 Shaft

We conducted Finite Element Analysis (FEA) on the solid model to enhance the accuracy of our design validation. FEA has been successfully used in designing FSAE car components [25]. The analysis focused on a static scenario, applying torque to the section of the shaft with a 1.181-inch diameter—directly connected to the engine. According to specifications, the maximum torque generated by the engine is expected to be 65 Nm. It's important to highlight that this torque value is effectively higher than what the engine will apply due to the anticipated installation of a 20 mm restrictor at the intake, which will reduce both power and torque output. In Figure 31, the 1.625-inch diameter section of the shaft was immobilized, and the static analysis was executed with a torque of 65 Nm applied to the rightmost side.

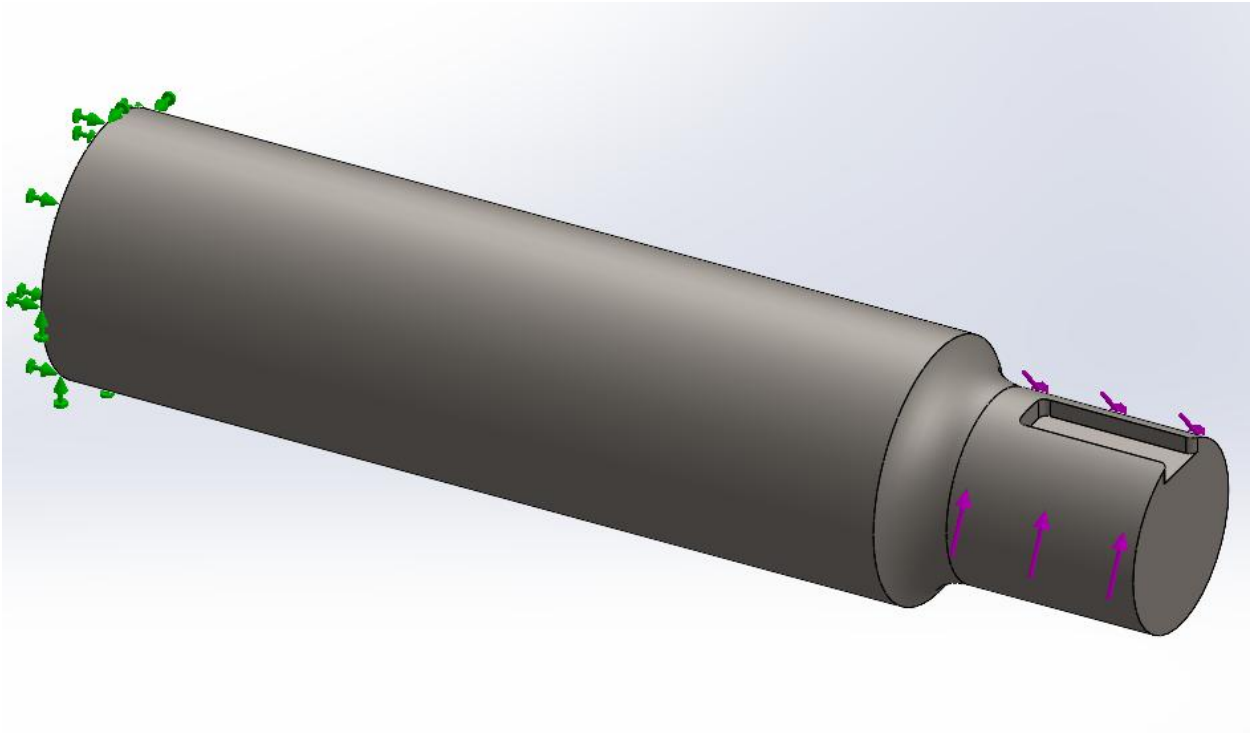

*Figure 31: Simulation model of shaft with both fixed and loaded ends shown*

Figure 31 illustrates the shaft being applied with a torque of 65 Nm from the engine in purple. It also illustrated the fixed end connected to the eddy current brake in green. A curvature-based mesh was used. The maximum element size was 0.5 inches, while the minimum element size was 0.0812516 in. Additionally, the total number of elements was 17210.

To ensure the accuracy of our results, we employed the h-adaptive method, an iterative technique. This method automatically refines the mesh in regions where the solution changes rapidly or demands high accuracy, while coarsening the mesh in areas where lower accuracy is acceptable. The adaptive meshing enhances the precision of simulation outcomes by concentrating computational resources where they are most crucial, optimizing computational efficiency. The vertical axis represents the resulting von Mises stresses incurred with each iteration, and the horizontal axis represents the analysis iteration that was performed. When the iterations converge toward a specific von Mises value, it can be reasonably assumed that the obtained results are justified.

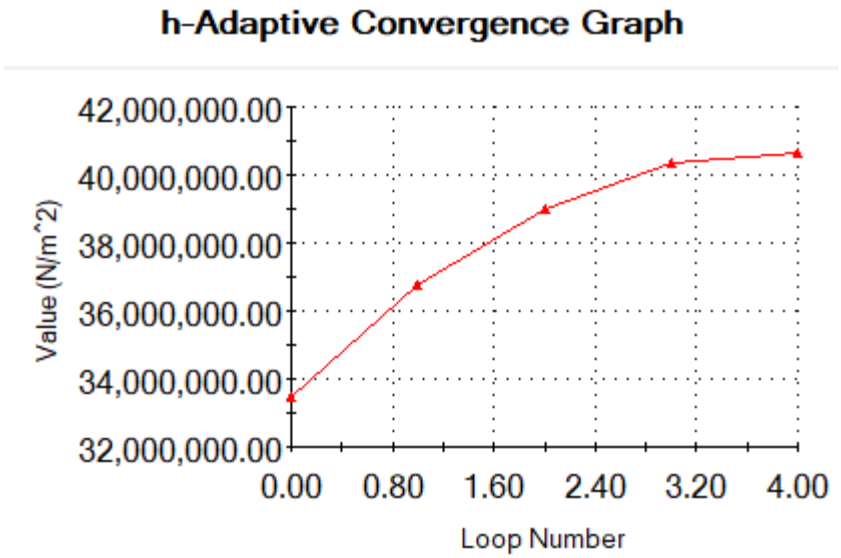


*Figure 32: h-adaptive graph*

Figure 32 shows the h-adaptive graph, which converges to approximately 40,500,000 N/m$^2$. The mesh size for the 4$^{th}$ iteration is 0.05 inches.

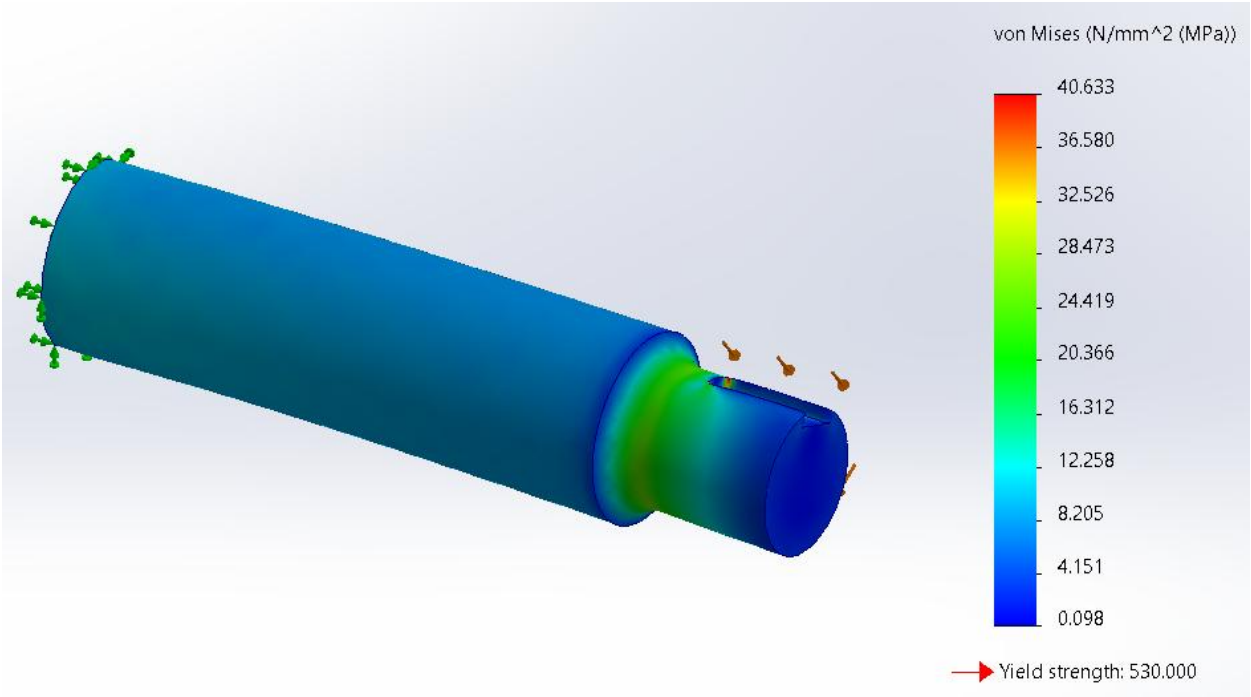


*Figure 33: Von Mises plot of shaft*

The von Mises plot illustrates that the highest stress applied to the shaft will be concentrated near the junction of the 1.18-inch and 2-inch segments. This outcome is expected, given the direct connection of this region to the engine. Identifying the location of this maximum von Mises stress is crucial for engineers to pinpoint critical areas in the design. The recorded critical von Mises stress is 30.281 MPa. The yield strength, denoting the stress a material can endure without undergoing permanent deformation, stands at 530 MPa for chrome-plated 1045 steel. A

noteworthy observation is the substantial difference between the von Mises stress and the yield strength. Specifically, the von Mises stress is orders of magnitude lower than the yield strength, a vital aspect in any engineering design.

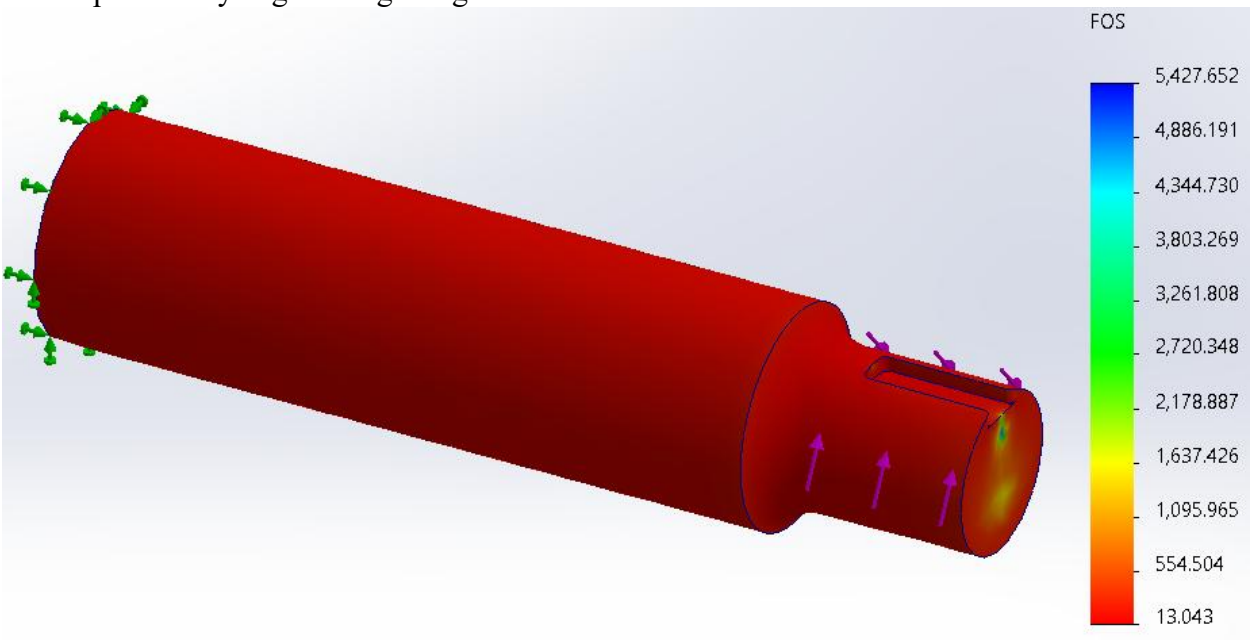


*Figure 34: Factor of Safety plot*

The Factor of Safety plot (Figure 34) serves as a complementary analysis to the von Mises plot. In the von Mises plot, the highest stress is documented at 30.281 MPa. By comparing this with the yield strength of 530 MPa, the Factor of Safety calculates a ratio, providing an assessment of the part's capacity to endure specified loads. The formula for this ratio is $FOS = \frac{Yield\ Strength}{von\ Mises\ stress}$. The region with the lowest factor of safety is the primary area of concern, and in this case, it coincides with the 1.18 / 1.625-inch connection region where the maximum von Mises stress occurs. At this vulnerable junction, the calculated factor of safety stands at 13.043. As stipulated earlier, a minimum factor of safety of 1.5 is required for safety standards. In this specific shaft analysis, the developed factor of safety comfortably exceeds this requirement, ensuring the component's reliability under specified loads. Therefore, reinforcing the location or enhancing the design for safety concerns is unnecessary.

### 4.1.2 Finite Element Analysis of Frame:

Performing an FEA on the frame with five fixed areas, representing the placement of five wheels, and three hundred pound (300lb) loads to on the pillow block stands to simulate the weight of the Eddy Brake, the maximum von Mises stresses determined were 18.528 MPa, which is quite small compared to the yield strength of the material, which is 325 MPa. The Factor of Safety determined was 17.541, which is significantly higher than the industry standard of 1.5. Based on the results from the FEA, the base section of the frame is viable for the project. Between the two 60-inch metal tubing, in the area where the engine is placed, there are two smaller rectangular areas made of 1.5 x 1.5 x 0.065 in.

### 4.1.3 FEA on the flanges:

Performing an FEA on the flanges confirmed the spacing and distance decision.

All flanges have their front edges chamfered to reduce the chance of injury when handling. The FEA was performed by adding fixtures to the bolt holes, representing braking by the Eddy Brake. A 65 Nm torque is applied between the center bore and a quarter-inch split area, which represents the torque that would be applied by the engine through the shaft. The split area represents the welded region. 65 Nm is the listed maximum torque produced by the engine to be tested. FSAE engines are mandated to have a restrictor to limit the output RPM. The von Mises stress determined was 3.066 MPa, which is far from the yield strength of 530 MPa. The factor of safety determined was 172.837, proving to be far above the minimum industry standard of 1.5.

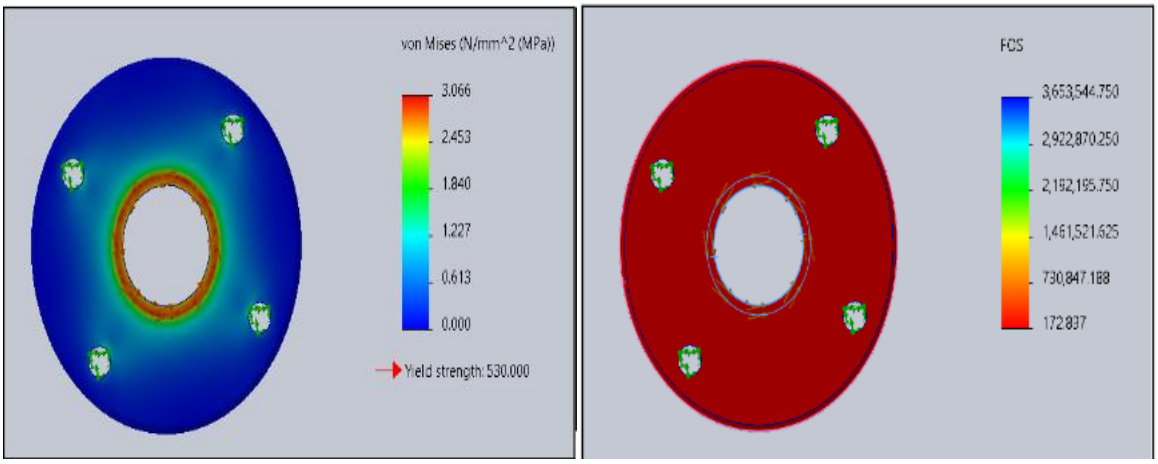


*Figure 35: Screenshots showing von Mises stresses (left) and factor of safety (right) from FEA performed on 6 in flanges*

Figure 35 shows the von Mises stresses(left) and the Factor of Safety(right) present when fix points are at the four bolt holes and a 65 Nm torque is applied between the edge of the center bore to 0.25in away from the edge of the center bore.

### 4.1.4 Finite Element Analysis of Load Cell Bracket

A FEA was performed on the structure using 220 N as the force applied to a circular region around the hole on the horizontal metal tube. This circular region represents a washer. 220N was the value used because 65Nm is the maximum torque that the engine can output. The distance of the circular region from the mounting face on the Eddy Brake is 4.5in or 11.4cm. The total distance from the circular region to the center of the Eddy Brake is 51.43cm or 0.5143m. Dividing this distance by the torque yields a force of 126.38N. Using 220N is a safe value as it is approximately 1.7 times the actual load expected. The three holes in which the bracket would be attached to the Eddy Brake remain fixed. A Factor of Safety of 3.850 was determined when 1010 was selected as the material. This material was the lowest grade steel possible within the given range, using SolidWorks. Maximum displayed von Mises stresses were 46.749 MPa. The values obtained from the FEA show the viability of using this material.

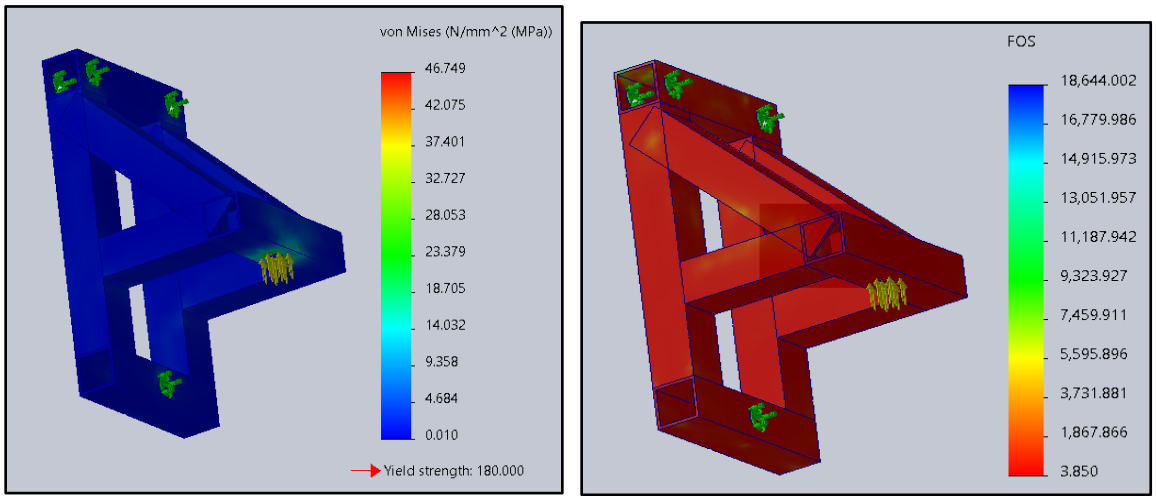


*Figure 36: Von Mises stress (left) and Factor of Safety (right) for initial design*

Figure 36 above shows the von Mises stresses and Factor of Safety charts for an FEA performed. Three fixed points are used, representing where the bolts would be used to fix the Load Cell Bracket on the Eddy Brake. An upward load of 220 N is applied to a circular split region surrounding the bolt hole.

In the final design, a slight change was made to the load cell bracket, removing the triangular section of the load cell bracket and replacing it with a horizontal metal tube, welded to the two vertical tubes. This decision was made because it better suited the space available for the load cell to be fixed onto the base plate.

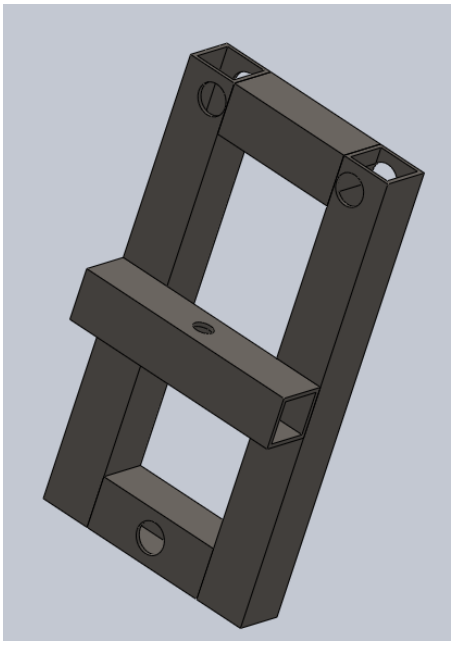

*Figure 37: Redesigned Load Cell Bracket*

Figure 37 above shows the redesigned Load Cell Bracket used for transmitting the torque from the engine, to a force acting on the load cell.

### 4.1.5 Finite Element Analysis of Support Rod

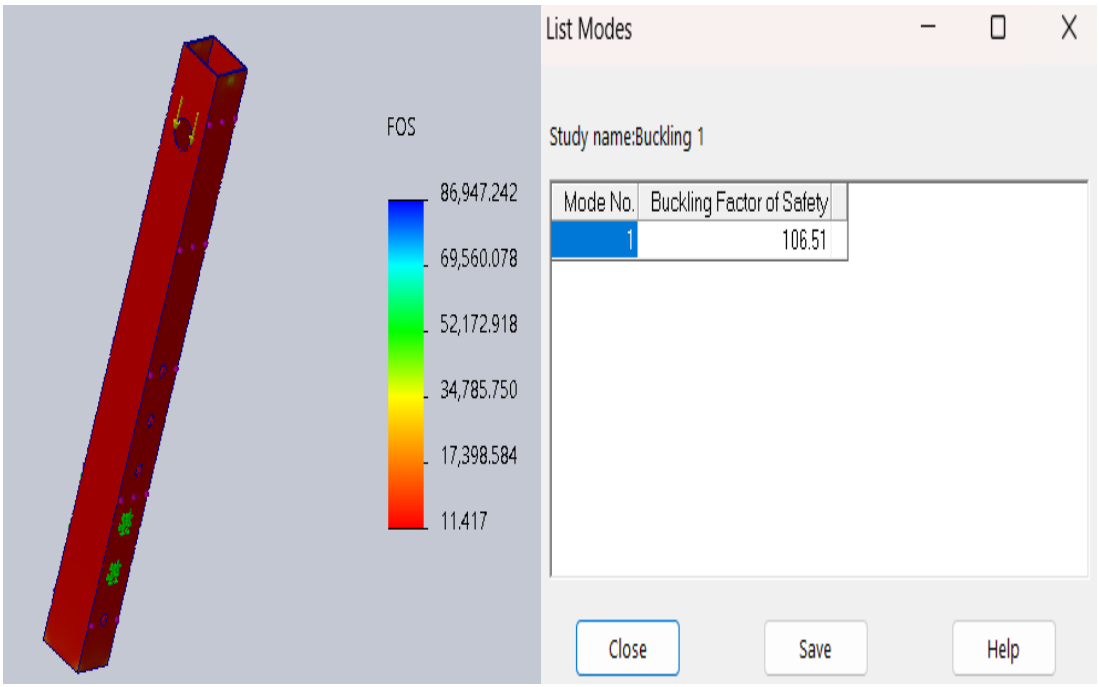


*Figure 38: FEA of rear mounts showing the Static study's Factor of Safety (left) and a Buckling Study Factor of Safety values (right)*

A factor of safety of 11.417 for a static analysis, exceeds the minimum allowable factor of safety of 1.5. A static study is primarily used to determine the stresses, displacements, strains and reaction forces within a structure under steady-state loading conditions. The buckling analysis deals with predicting the critical loads at which a structure would likely undergo buckling. Buckling is a sudden and catastrophic mode of failure. This particular part was the basis of our study for the rear mount as it has the largest surface area on which the load is applied, while the overall area of the metal tubing is the smallest. The outer tube would be able to withstand higher loads as it has a larger surface area. Also, the inner tube is slender and longer than the outer tube.

### 4.2 Final Assembly for Fabrication

After the FEA analysis on critical components, the assembly was finalized for the fabrication processes. The finalized assembly is shown in Figures 39 and 40.

Final Design and assembly drawing:

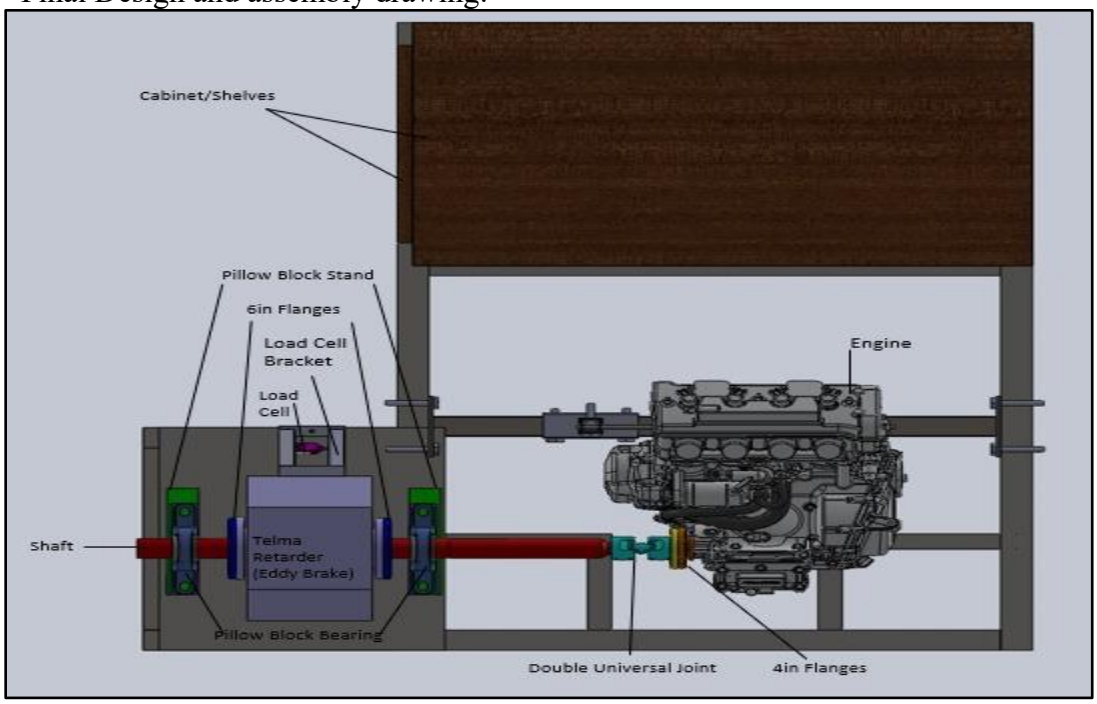


*Figure 39: Top View of Engine Dynamometer Assembly*

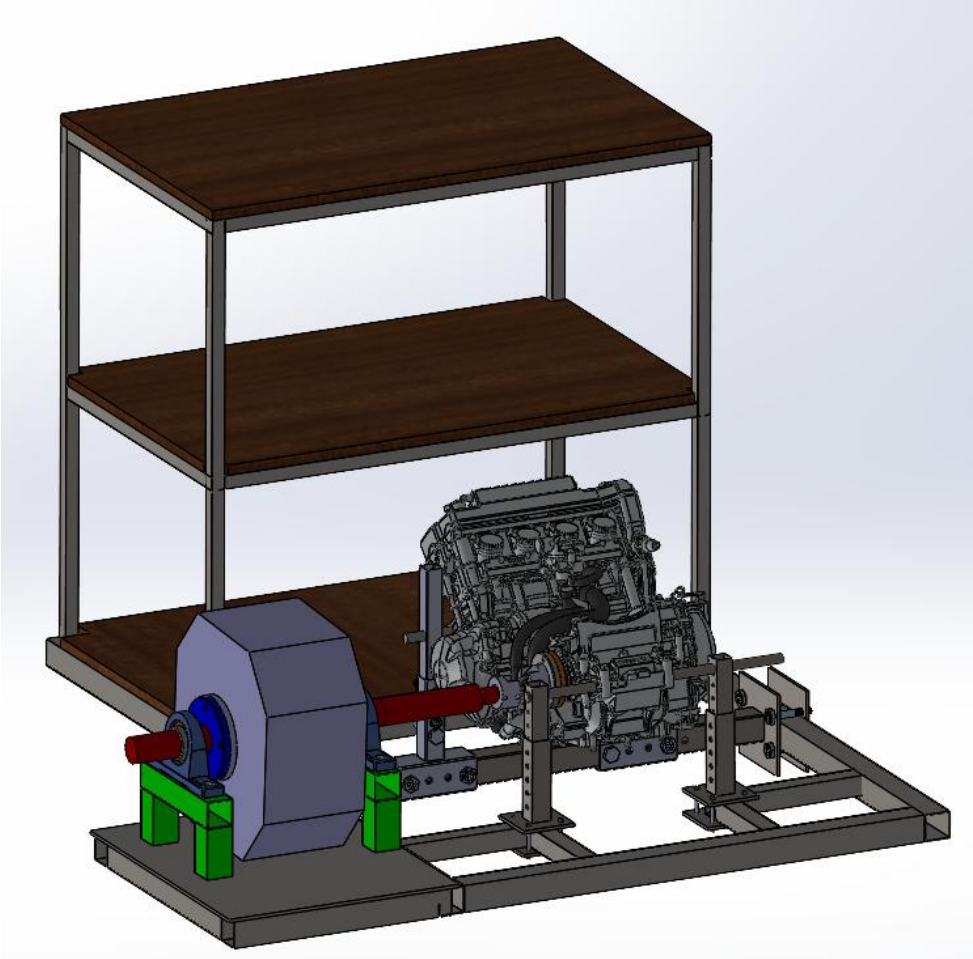

*Figure 40: Isometric View of Engine Dynamometer Assembly*

**4.3 Fabrication:**

Different steps were taken for the fabrication of the assembly. The steps are described in detail below.

**4.3.1 - Dismantling Eddy Current Brake**

We started this process by identifying all parts before dismantling in order to find initial operations during the re-assembly. We removed the bracket that is in the main connecting block on the right of the eddy brake.

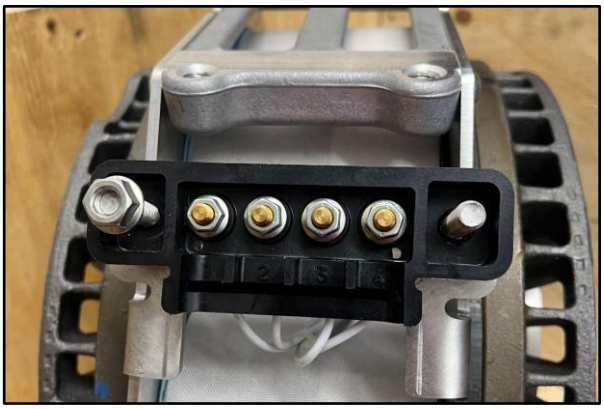

*Figure 41: Connecting Block Side*

On the eddy brake axial side, we removed the lock tab by using a flat screwdriver and slowly began to try the removal of this.

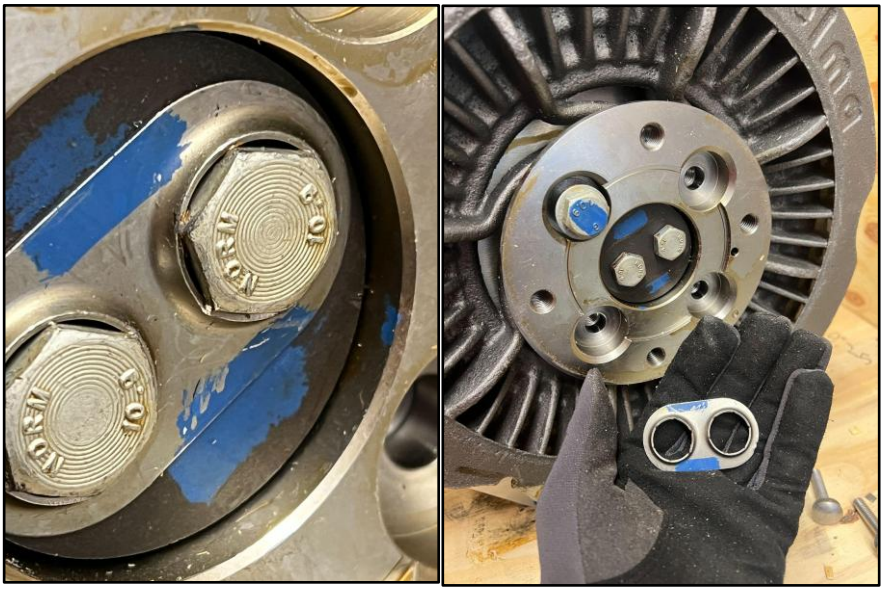

*Figure 42: Lock Tab (left) and Lock tab off the end shaft plate (Right)*

The two end shaft screws had to be removed using a 17mm socket and a bar to lock the rotation of the motor. The 2 end shaft screws with the end shaft plate will come off.

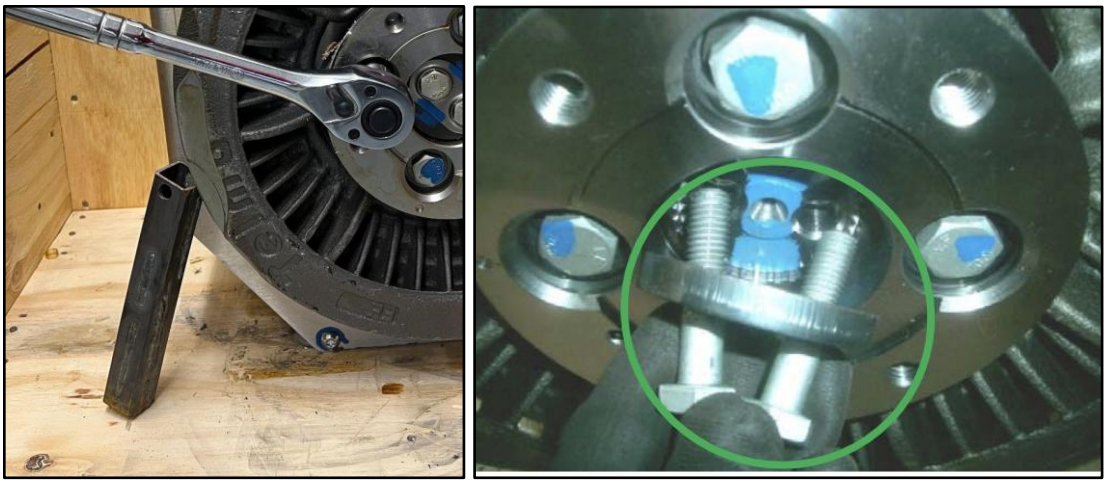

*Figure 43: Bar to lock the rotation (left); Shaft screws taken off (right)*

The rotor with the coupling flange will come off, removing the dust shield from the shaft line.

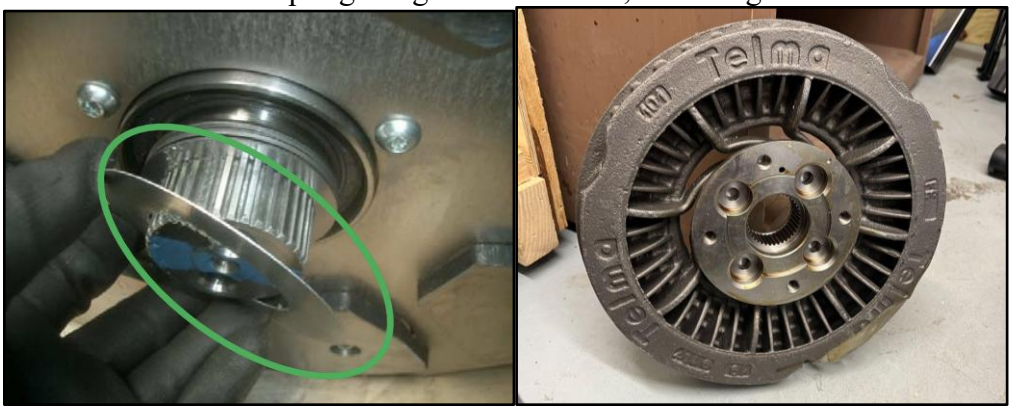


*Figure 44: Coupling flange (left); Rotor (right) taken off*

Unscrewing the 2 nuts and 2 washers securing the cover to the connecting block, and removing them using a 10 mm long socket. Then the cover would come off.


*Figure 45: Connecting block taken off the starter frame*

Unscrewing the nut securing the connecting block to the stator frame, isn't necessary to remove the nut completely. Using a 10 mm long socket.

Unscrewing and removing the 15 screws securing the pole shoes plate to the fixation pads, poles and hub using a T-40 wrench to unscrew the 15 screws.

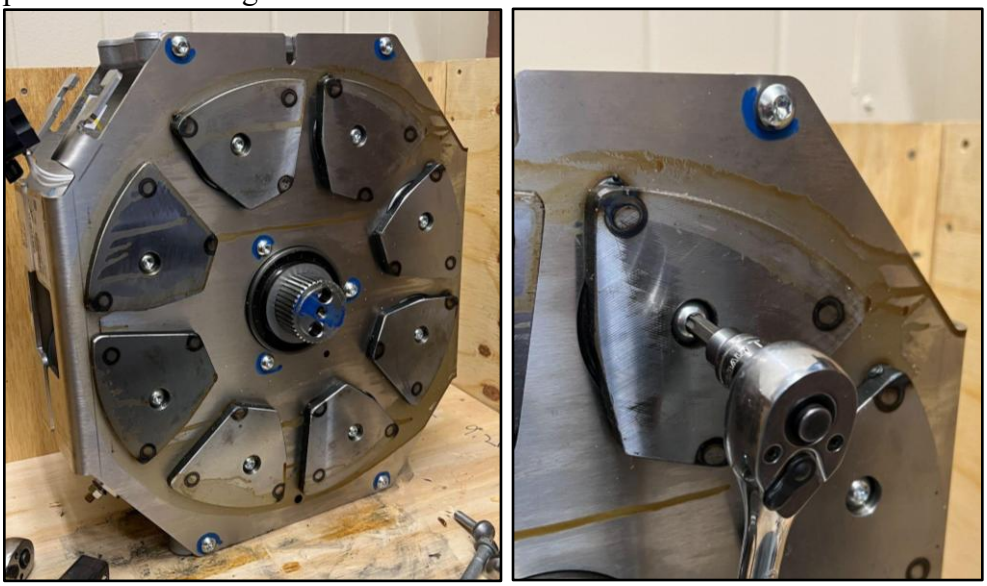

*Figure 46: Pole shoe plate (left) and removing screws from pole shoe plate (right)*

Slowly begin to lift the pole shoe plate and remove it completely. Now you will have a view of the retarder with the pole shoes plate removed.

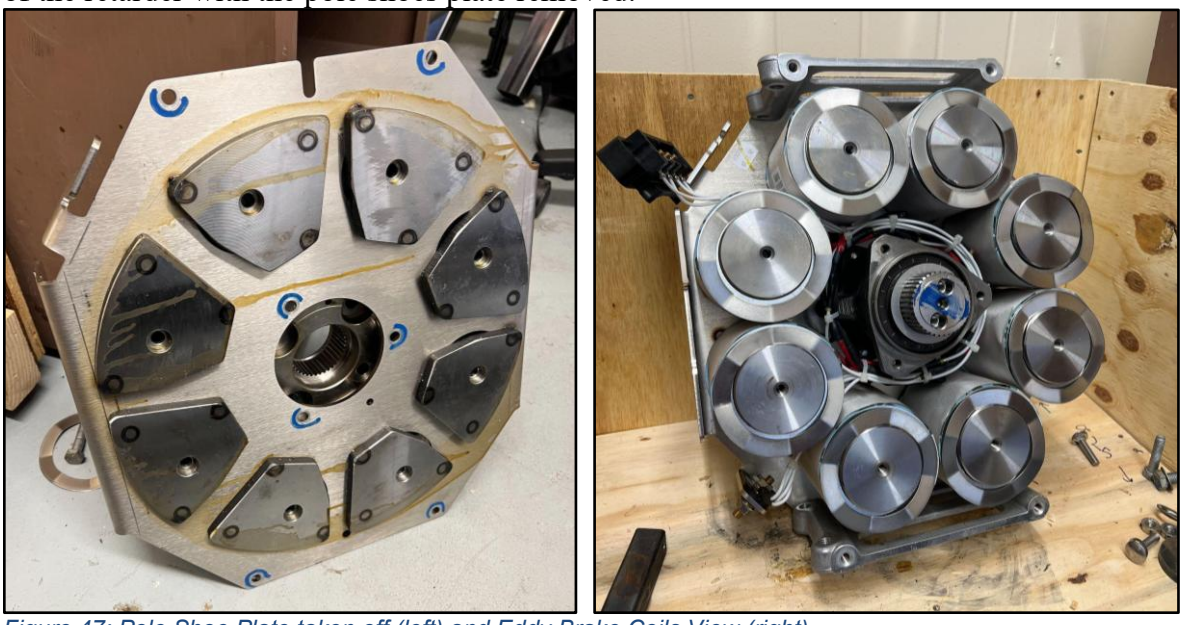

*Figure 47: Pole Shoe Plate taken off (left) and Eddy Brake Coils View (right)*

Now we carefully follow the wiring diagram and begin to rewire. Marking the first set of coils with a sharper we can follow the wires pattern.

*Figure 48: Internal Wiring (left) and Wiring traceability (right)*

We made sure we follow the coils pattern, ensuring that the north and south poles are adjacent to create opposing magnetic fields, the system optimizes the generation of eddy currents. The unique approach of folding and wrapping one end of the wire to align with the other end enhances the uniformity of the coil configuration. All the coils are wound the same, and instead of having one wire at each end of the coil, the way these were wound is that one of the ends of the wires is wrapped and folded to the side of the coil so the wire ends at the same end as the other.

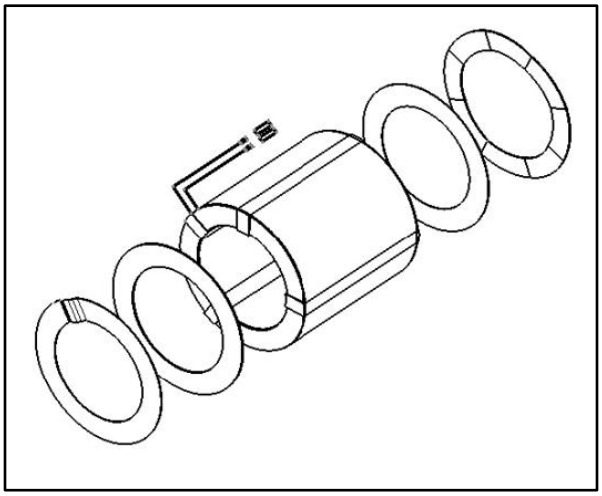

*Figure 49: Coil Diagram*

Carefully cut the zip ties so the wires can move freely to better perform the cutting of the wires.

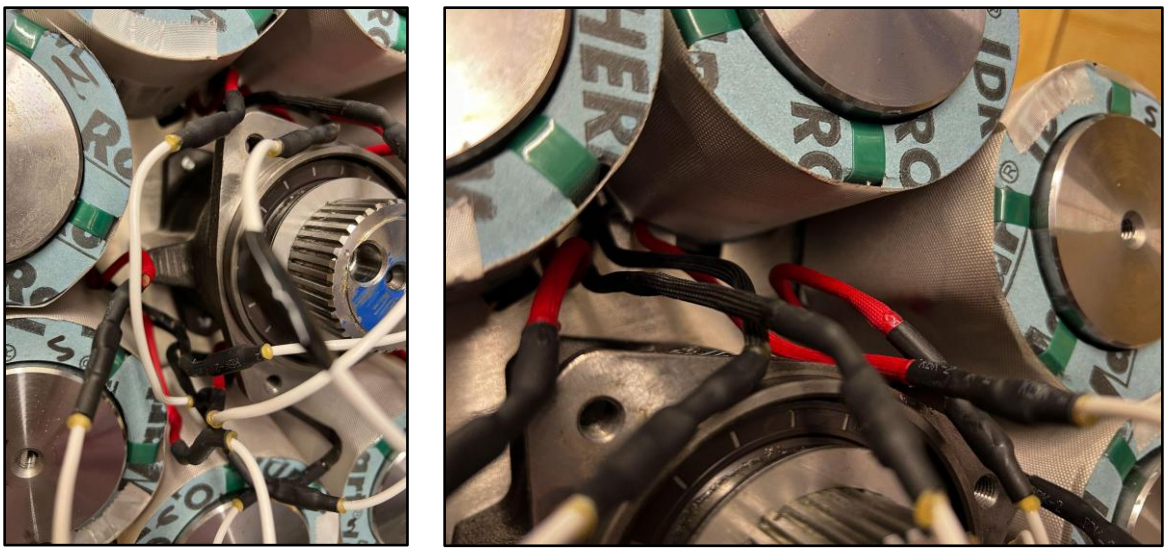

*Figure 50: Wires without zip tie (left) and Positive and Negative wires (right)*

We alternate the direction of the current with the following coil next to each other so this configuration can be in series and still provide eddy currents. Once we've performed the wiring process, the results will show in the following.

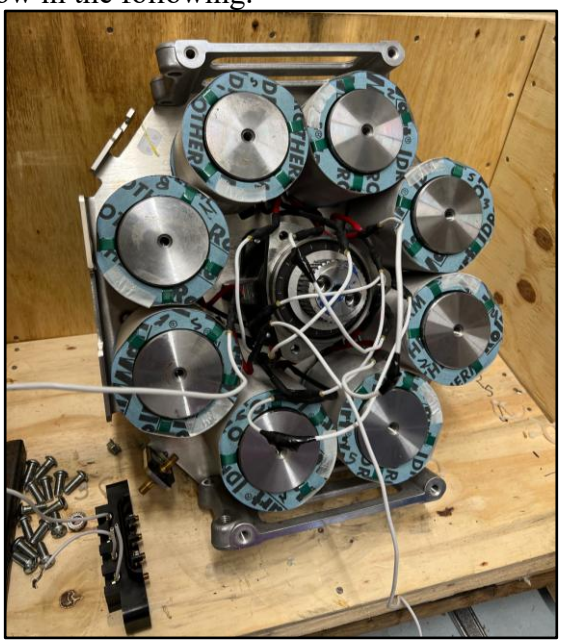

*Figure 51: Wiring Configuration in Series*

Then carefully re-arrange the wires and zip tie them to organize the wiring stages. Once this is complete, make sure to carefully put every part of the eddy brake back together.

### 4.3.2 - Powering the eddy brake

A robust and reliable power supply was fundamental to the success of our eddy brake. In this case, it served as the backbone that supported all our operational functions. Our initial power setup included a configuration of four 12V batteries connected in series, a DC to AC inverter, and an

eddy brake power supply. However, before powering up the system, it was essential to ensure safety and correctness in the installation, including the eddy brake. A certified electrician was consulted, providing the necessary feedback and approval to proceed. After we ensured that all components were properly installed and checked by a certified electrician, we proceeded to activate the eddy brake system. Based on our theoretical calculations and design specifications, we confidently adjusted our power supply to output the necessary voltage to power up the eddy brake. This step was crucial because it directly influenced the effectiveness of the eddy brake functionality. We successfully observed the eddy brake operating as expected, demonstrating the practical application of our theoretical understanding and confirming the systems capabilities in real-world conditions. Upon activation, the eddy brake was able to run for about 30-45 minutes; this was due to insufficient power from our initial setup, prompting the switch to a different method. We decided to switch to a generator as a power supply for our setup. This change allowed for continuous operation of the eddy brake, confirming its functionality and readiness for further testing.

### 4.3.3 - Frame Fabrication

The picture in Figure 52 below shows the completed frame with wheels and swivel stands installed and base boards for cabinets fastened. The cabinet section is almost complete. It requires finishing carpentry work and cosmetic improvement.

*Figure 52: Current Frame with cabinet bases and wheels installed*

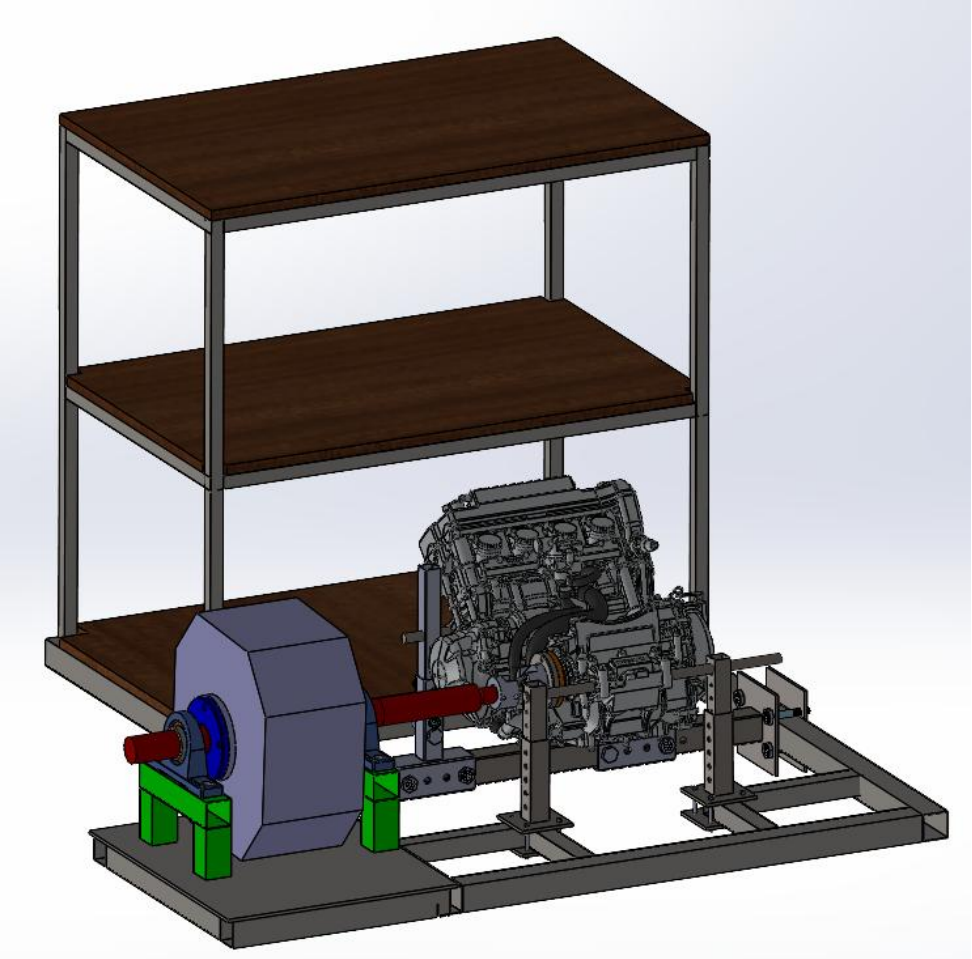

*Figure 53: Isometric view of the Engine Dynamometer Assembly*

Figure 53 shows an isometric view of the engine dynamometer assembly, with newly designed components colored.

**Red -** On the left is a 6in long shaft which is idle. It doesn't transmit any torque. Its sole purpose is to hold the Eddy Brake suspended over the base plate, allowing it to rotate. On the right is a longer shaft which transmits torque from the engine to the Eddy Brake. It is attached to a 6in flange on the left and a Double Universal Joint on the right.

**Dark Blue -** Two 6in flanges are colored blue. These flanges allow attachment of the shafts to the Eddy Brake. Their fastening holes are not threaded and rectangularly patterned. This feature corresponds to the threaded rectangular holes built into the Eddy Brake's flanges.

**Light Blue -** Pillow Block Bearings: They allow rotation of the shafts, while supporting the weight of the Eddy Brake, Shafts and Load Cell Bracket.

**Green -** Pillow Block Stands: They support the weight of the Eddy Brake, Pillow Block Bearings, Shafts and the Load Cell Bracket. They keep the Eddy Brake suspended.

Teal- Double Universal Joint: It is attached to the (drive)shaft on one end, and to a 4in flange on the other end. It is used to compensate for misalignment between the shaft and the engine's output shaft.

**Yellow -** 4in Flange "Double Universal Joint Side": It allows a connection between the Double Universal Joint and the engine "Sprocket Side" 4in Flange. It has a through cut in the center with

a diameter of 2.30 in. This cut allows the Double Universal Joint to be fitted inside of the flange for welding. The bolt holes are symmetric holes with no threading, allowing the fitting of a 5/16 in bolt through it.

**Orange -** 4in Flange "Sprocket Side": It allows a connection between the engine's output shaft and the Double Universal Joint, through the Double Universal Joint Side 4in Flange. It has a through cut 1.5in in diameter. This cut allows the partial insertion of a sprocket which is welded onto the flange. Its bolt holes are symmetric with 5/16-18 threading inside, allowing connection from the Universal Joint Side 4in Flange.

**Brown -** Shelves: Three shelves are built into the frame. They are used to store a fuel tank and electrical components such as batteries. The top shelf is used to shelve the operator's display devices and computer.

### 4.3.4 - Component Fabrication

The manufacturing process involved utilizing the lathe, drill press, and Metal Inert Gas (MIG) welding machine. Mr. Jay Barnett and Mr. Frank Bohuslav operated the lathe, while classmate Kory Prather managed MIG welding. The lathe was employed to reduce the diameter of the 1⅝ inch shaft in specific sections and to cut through the cross section of the flanges. Welding played a prominent role in the manufacturing process, and its details are outlined below.

#### 4.3.4.1 Sprocket to 4-inch flange

*Figure 54: Sprocket welded onto flange*

As seen in Figure 54, a sprocket is welded onto the flange. This particular sprocket is from JT sprockets with a part number of JTF 1370. Its dimensions are seen in Figure 55 below.

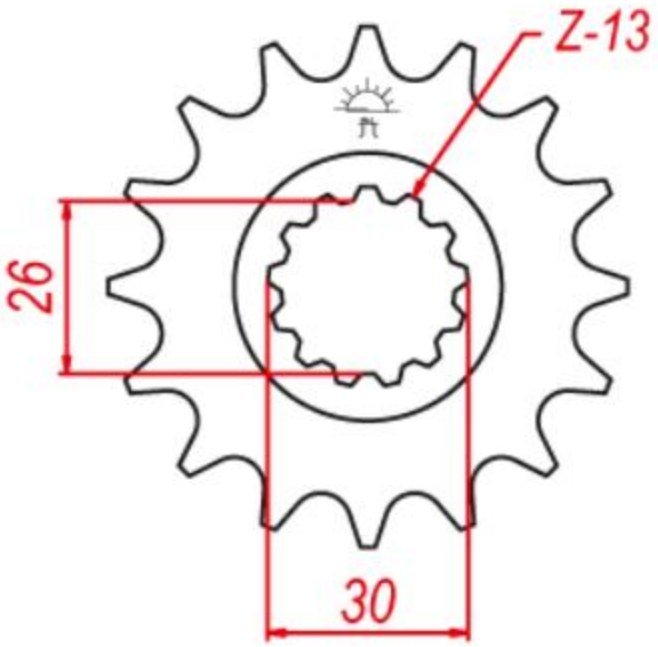


*Figure 55: Dimensions of engine sprocket*

The engine sprocket served the purpose of linking to the engine's crankshaft before being welded onto a flange, which acted as an adapter for our double universal joint. Although the sprocket teeth on the flange were unnecessary for our design since we weren't utilizing a chain for power transmission from the engine to the dyno, they remained intact. In hindsight, it might have been preferable to cut out the teeth for a smoother finish, but this was omitted to streamline the manufacturing process and minimize lead time.

#### 4.3.4.2 Flange to shaft

*Figure 56: Rotary shaft welded onto flange*

This shaft is welded onto a 6-inch flange that is to be connected onto the rear side of the eddy brake as seen in figure 57 below

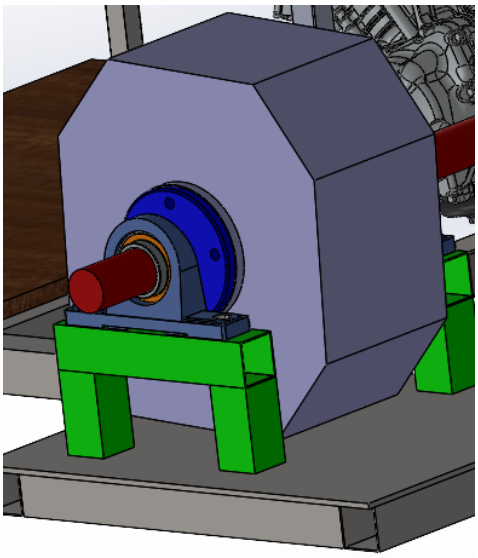

*Figure 57: Model highlighting where this rotary shaft is to place in the assembly*

The purpose of this component is to aid in the suspension of the eddy current brake, while it is in rotary motion.

#### 4.3.4.3 Double universal joint to flange

*Figure 58: Double Universal Joint welded onto 4-inch flange*

This dual universal joint, procured from HUCO, ensures safe operation at speeds up to 6000 rpm. Its primary function is to accommodate any misalignment between the main rotary shaft connecting the eddy current brake and the engine. Welded onto a 4-inch flange, the double universal joint facilitates seamless integration with the sprocket. The decision to attach the sprocket was straightforward, as there was ample clearance on the engine side. However, the placement of the pillow blocks supporting the eddy current brake imposes constraints on the length of the U-joint that can be utilized. Additionally, opting to attach the U-joint in the middle would necessitate the fabrication of two separate shafts, resulting in material wastage and increased manufacturing time.

#### 4.3.4.4 Flange to main rotary shaft:

*Figure 59: 6-inch flange welded to main rotary shaft*

This was produced following the precise steps depicted in Figure 59 above. Serving as the primary rotary shaft, it transfers power from the engine to the eddy current brake. Power transmission is facilitated by a key positioned within the keyways of both the shaft and the double universal joint. Although not easily discernible in Figure 60 upon cooling, the weld caused a slight misalignment of the shaft relative to the flange, resulting in a minor angular distortion.

**4.3.4.5 Pillow block stands:**

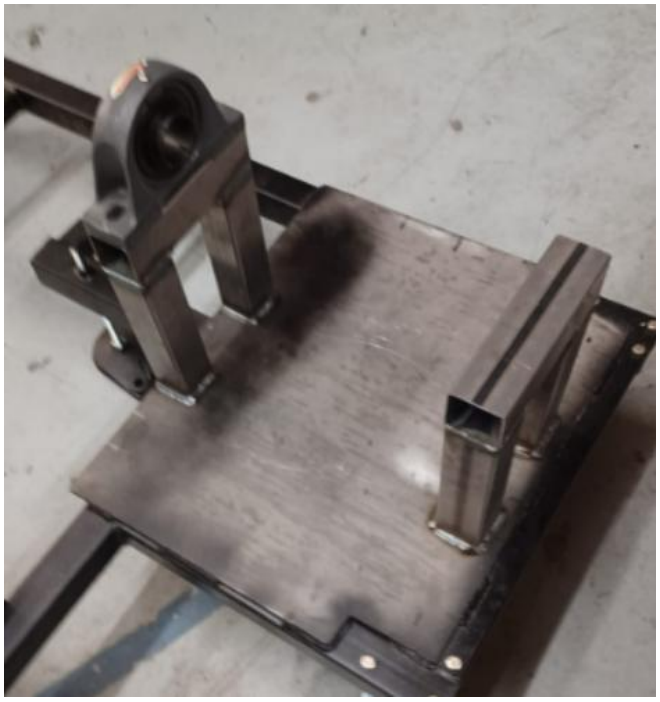

*Figure 60: Pillow block stands welded to frame*

Figure 60 illustrates the placement of the pillow block stands, welded onto the frame to ensure alignment with the plate depicted above. These stands serve as the mounts for the pillow block bearings, which bear the forces exerted by the rotary shafts. Once again, the presence of these stands is crucial for suspending the eddy current brake. This suspension setup enables the attachment of a load cell in a manner that engages with the resistive rotation of the eddy brake. Additionally, this arrangement facilitates improved heat dissipation, particularly since we are utilizing two high-heat generating devices.

#### 4.3.4.6 Load cell bracket

Five sections of rectangular tubing were cut to the desired size for welding. Two longer pieces are used vertically, two short pieces join the vertical pieces on the top and bottom, creating a rectangle. The fifth section is 2in longer than the two short sections and is welded midway across the two longer sections. Welding is performed on both the top and bottom corners this fifth tube. Measured. After welding, mounting holes were drilled in order to mount the load cell bracket onto the frame.

### 4.3.5 Final fabricated assembly


*Figure 61: Final fabricated product of engine dynamometer*

The final fabricated engine dynamometer has all fabricated components fixed in place with bolts, nuts and washers. The fuel tank is the only component not fixed in place at this point as the original fuel tank had to be removed due to leaks. From this angle(rear), the rear mounts can be seen with a horizontal shaft positioned in them, holding the engine in place. A section of the double universal joint and shaft can be seen connecting the engine to the eddy brake, on both sides of the eddy brake(left), pillow block bearings sit on pillow block stands which are welded to the frame. The eddy brake is suspended over the base plate. On the top shelf, a computer is seen. This computer is used to communicate with the engine via the ECU and to modify the voltage input via an Arduino. On the top right, an emergency push button (stop button) is seen. On the left side of the computer, a section of the gear shifter lever can be seen. In the left-middle section, a generator is seen. This generator provides a steady 220-240V AC with a maximum current output of 30A.

### 4.4 Test Results: (Results of test after running the dyno)

Figure 62 below shows the interface of the ECU as seen from the laptop.

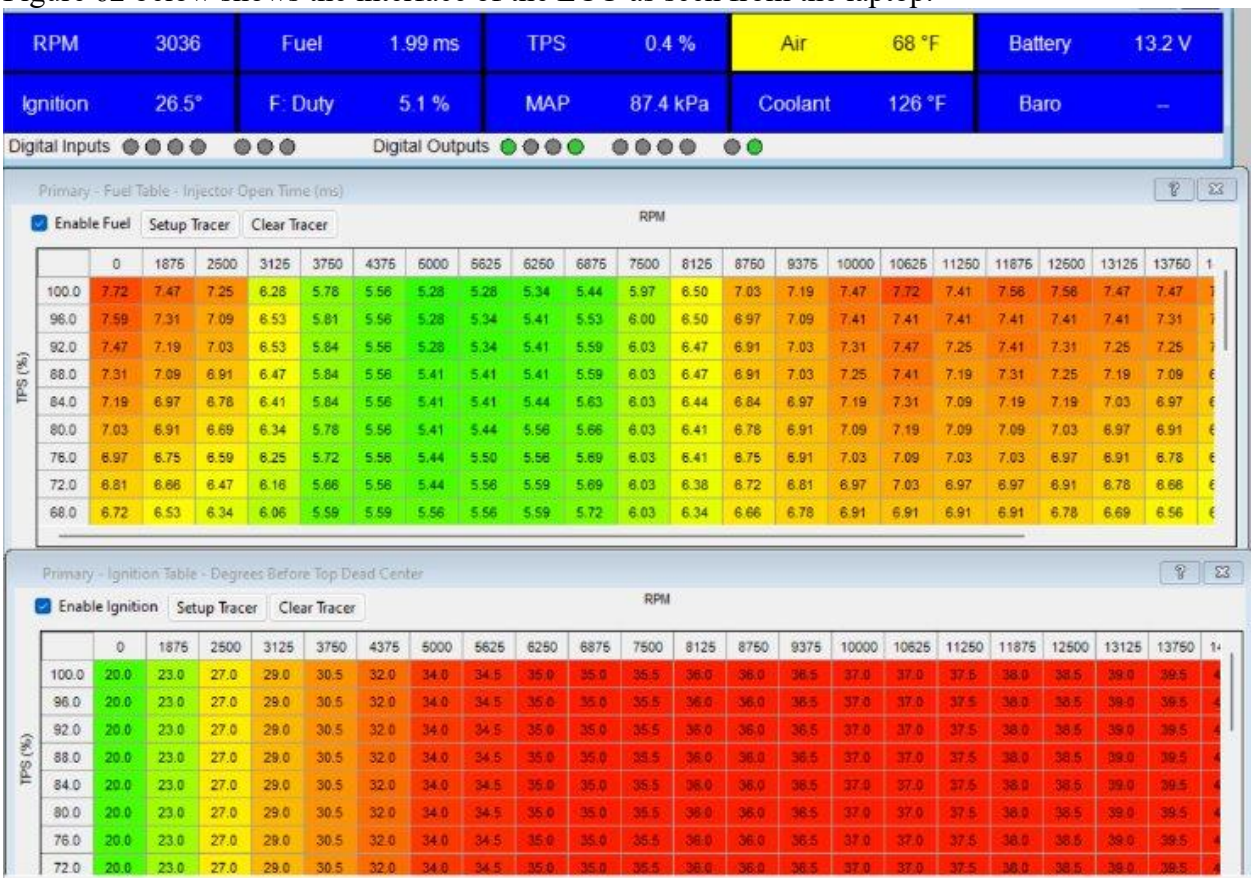


*Figure 62: Interface of PE₃ ECU*

The top blue cells display real-time engine data while the engine is operational. Each data point within these cells requires calibration, following the guidelines outlined in the PE3 user manual. The fuel table delineates cells aligned with specific RPMs and throttle positions, dictating when fuel injectors are activated to release fuel into the cylinders. Similarly, the ignition table features cells corresponding to particular RPMs and throttle positions, dictating the timing of ignition events relative to top dead center. Both the fuel and ignition tables are editable in real-time, allowing for optimization of engine performance as other hardware parameters are adjusted.

Once the engine is running, data can be gathered through the 'Trigger Diagnostics' table. The data observed shows the length of time of activations as seen in figure 63 below:

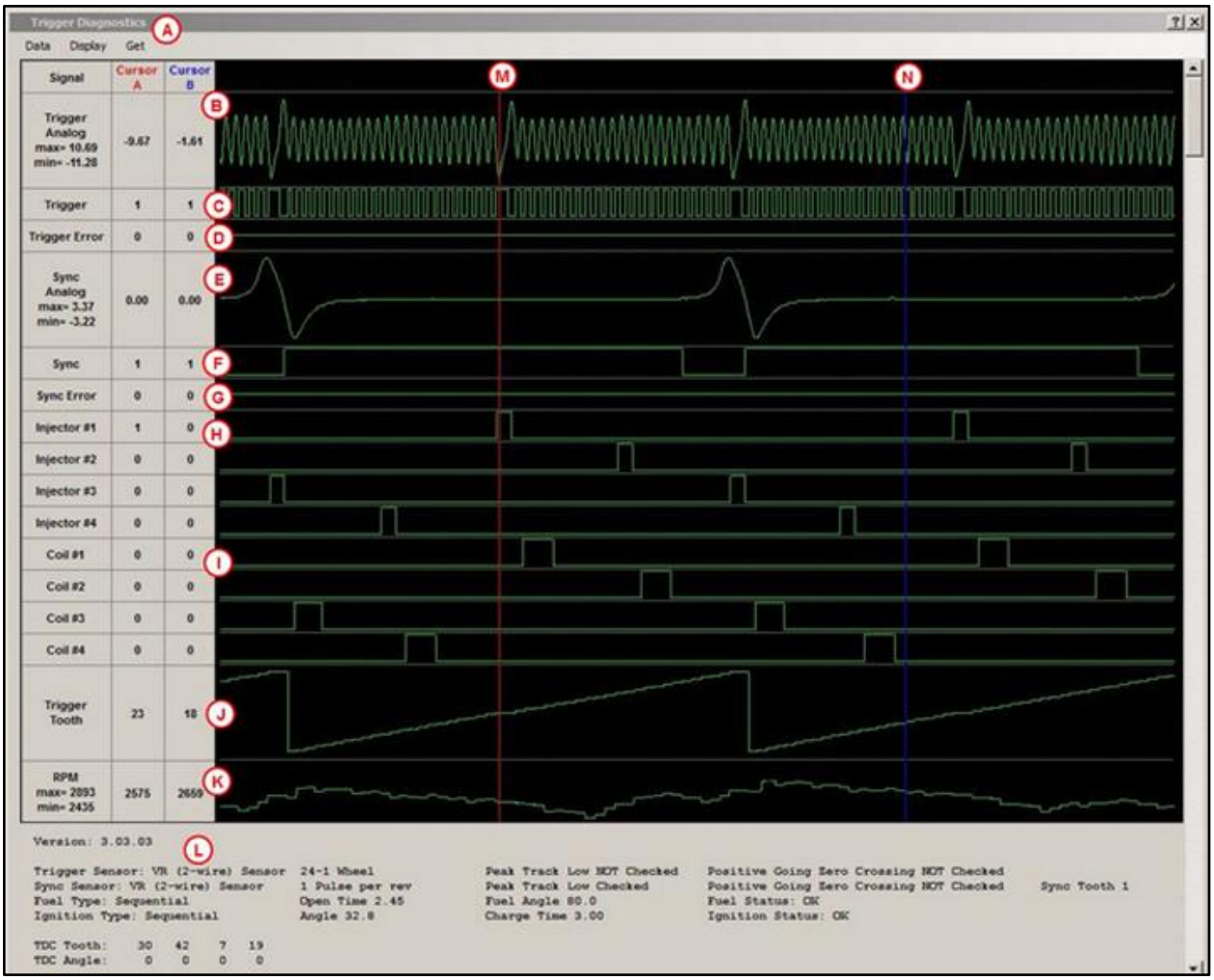


*Figure 63: Timing data from output devices from engine*

**A**:

The drop-down header contains options for getting, saving and viewing data. See below for a description of each command.

**Data** - This contains commands for collecting, loading and saving data from trigger diagnostics.

- Get = 'Get' forces the PE3 to collect data based on the current configuration settings, regardless of an RPM signal being detected. While the ECU is collecting data, peMonitor will pause for a moment to gather the data.
- Auto Trigger = This arms the trigger diagnostics such that data was collected as soon as an RPM signal is detected. In order for RPM to be calculated by the PE3, the ECU must be receiving trigger and sync signals consistent with the way the ECU is configured. If a 'Crank Error' is present, RPM will not be calculated.
- Save to a file = This command saves the currently displayed trigger diagnostic data to a .peDiag file that can be loaded and viewed at a later date.
- Read from a file = 'Read from a file' allows the user to load previously stored .peDiag data from disk.
- Extract analog data = This function extracts the raw Trigger and Sync voltage data from the window and allows the user to save it in a comma-separated variable (CSV) file.

- Zero RPM Sample Rate = This parameter sets the trigger diagnostic sample rate when a valid RPM is not present (RPM=0). This determines how quickly the PE3 collects data. The sample rate can be set to high, medium or low. A low sample rate provides a longer data trace (more revolutions) but sacrifices resolution. A high sample rate provides a shorter window of data in time but at higher resolution.
- Valid RPM Sample Rate = This parameter sets the trigger diagnostic sample rate when a valid RPM is present (not zero). This determines how quickly the PE3 collects data. The sample rate can be set to high, medium or low. A low sample rate provides a longer data trace (more revolutions) but sacrifices resolution. A high sample rate provides a shorter window of data in time but at higher resolution.

**Display** -This includes commands and settings for displaying trigger diagnostic data.

- Redraw = This redraws the plotted data in the graph.
- Zoom In = 'Zoom In' zooms in to the data between the cursors.
- Zoom Out = This command expands the plot out.
- Hide Injectors = 'Hide Injectors' hides the injector traces on the data plot. This shortens the overall window height to make it easier to display on small monitors.
- Hide Coils = 'Hide Coils' hides the coil traces on the data plot. This shortens the overall window height to make it easier to display on small monitors.
- Move Cursor A = Cursor 'A' (the red cursor) can be moved by dragging it with the mouse or by using the right and left arrow keys.
- Move Cursor B = Cursor 'B' (the blue cursor) can be moved by dragging it with the mouse or by holding the Shift key and using the right and left arrow keys.

**Get** - 'Get' forces the PE3 to collect data based on the current configuration settings regardless of an RPM signal being detected. While the ECU is collecting data, peMonitor will pause for a moment to gather the data. This is the same as 'Get' under the drop-down menu 'Data' above.

**B:**

This segment of the plot represents the analog signal received as the trigger input. In the illustrated scenario depicted in the figure, it corresponds to a 24-1 tooth crank wheel employing a 2-wire, variable reluctance sensor.

**C:**

This represents the digital transformation of the trigger analog signal post-signal conditioning in the PE3. This processed signal is what the processor within the ECU detects. The processor specifically identifies a rising edge in this signal (transition from 0 to 1) for its operation.

**D:**

The 'Trigger Error' indicator activates when there's an error detected in the trigger signal. Whenever an error occurs, this indicator switches to 1 from 0. Both trigger errors and sync errors contribute to the overall 'Crank Error' status displayed on the main peMonitor screen.

**E:**

This section of the plot represents the analog signal corresponding to the sync input. In the depicted scenario, it pertains to a single tooth signal that occurs once per engine cycle, employing a 2-wire variable reluctance sensor.

**F:**

This digital signal mirrors the sync analog signal once it undergoes signal conditioning in the PE3. This processed signal is what the ECU's processor perceives. Specifically, the processor relies on a rising edge (transition from 0 to 1) in this signal for its operations.

**G:**

The 'Sync Error' indicator is activated when there's an error detected in the sync signal. Whenever an error occurs, this indicator switches to 1 from 0. Both trigger errors, sync errors, or both contribute to the overall 'Crank Error' status displayed on the main peMonitor screen.

**H:**

This plot row illustrates the opening and closing of injectors. In the depicted scenario, four injector drivers are utilized, one dedicated to each cylinder. When this signal shifts from 0 to 1, it indicates that the injector has opened.

**I:**

This section of the plot displays the charging and firing of ignition coils. In the illustrated example, four ignition drivers are employed, each assigned to a cylinder. A transition from 0 to 1 indicates that the coil is charging, while the coil fires when the signal shifts from 1 to 0.

**J:**

The 'Trigger Tooth' plot monitors the current trigger tooth within the data. In the displayed scenario, the trigger tooth progresses from 1 to 46. This progression occurs because the engine utilizes a 24-1 tooth profile trigger wheel (comprising 23 teeth). Since the engine operates with a sync signal and adopts a 'cycle-based' reference frame, the trigger tooth increments over two crank revolutions, spanning from 1 to 46.

**K:**

This row in the plot shows the instantaneous engine RPM for every trigger tooth in the data.

**L:**

The section beneath the plot provides supplementary details regarding the engine and its configuration at the time the trigger diagnostic plot was generated. This information is also stored in the peDiag file if the data is saved to disk.

**M:**

This is 'Cursor A'. It can be moved through the data by clicking and dragging with the mouse or by using the left and right arrow keys.

**N:**

This is the blue cursor, 'Cursor B'. It can be moved through the data by clicking and dragging with the mouse or by holding the shift key while using the left and right arrow keys.

## 5 Conclusions:

### 5.1 Summary

As we conclude this phase of our senior design project, we are thrilled to present the culmination of our dedicated efforts in advancing automotive engineering testing capabilities through the comprehensive design and integration of an engine dynamometer system. Our journey has been one of meticulous research, innovative design decisions, and precise execution, all aimed at pushing the boundaries of what's possible in automotive testing.

At the heart of our dynamometer system lies the sophisticated AF50-90 retarder, meticulously selected for its superior performance and compatibility with our dynamic testing needs. This choice was informed by a thorough exploration of theoretical principles and configurations, including coil winding patterns and series arrangements, ensuring optimal functionality and reliability. Complementing this core component are various electrical elements, including an AC generator, eddy current power supply, and the AF50-90 retarder, seamlessly integrated to form a robust power supply system capable of meeting the demanding requirements of our testing scenarios.

Our design process was characterized by a careful balance between theoretical considerations and practical constraints. Utilizing advanced software such as SOLIDWORKS, we meticulously crafted the structural components of our dynamometer system, ensuring both functionality and durability. The completion of manufacturing processes for crucial components like flanges, mounts, and shafts further underscored our commitment to excellence, guaranteeing the physical integrity of our system.

Moreover, we embarked on the critical task of modifying the engine's wiring harness to ensure seamless compatibility with our dynamometer setup. This meticulous attention to detail extended to the integration of a Data Acquisition system, meticulously calibrated to retrieve data from an array of sensors, enabling precise and comprehensive dynamic testing.

Executing this feat required the direct application of engineering economics. For every decision made, the cost of raw materials, time for fabrication and the total budget was considered. Before purchasing raw material, simulations performed were used to validate decisions. We ensured that the functionality of the final product, its safety standard and durability were considered when selecting items for purchase. Spending time researching, designing, simulating and discussing allowed us to reach milestones, while being prudent with our budget.

As we celebrate the assembly of our Engine Dynamometer, we reflect on the countless hours of dedication and teamwork that have brought us to this point. This milestone represents the culmination of months of hard work, innovation, and problem-solving, positioning our dynamometer system as a pioneering force in the realm of automotive testing.

### 5.2 Future Work

In the pursuit of continual improvement and ensuring the highest standards of safety and performance, several key areas have been identified for future development and enhancement. This comprehensive plan encompasses various aspects ranging from safety measures to performance optimization, all aimed at elevating the capabilities and reliability of our system.

Safety is paramount in any endeavor, especially in high-speed applications such as Formula SAE. Therefore, one of the primary focus of our future work involves the implementation of complete safety measures. This encompasses a multi-faceted approach, including the integration of automated emergency shutoff systems and limiters based on threshold signals. These measures are designed to automatically respond to potential hazards, safeguarding both the vehicle and its occupants.

Another critical aspect to address is the mitigation of vibration. Excessive vibration can compromise the performance and longevity of various components. We will start by evaluating the susceptibility of critical vehicle components to vibration-induced stress, leveraging our understanding of vibration profiles. Following this assessment, we will employ isolation and dampening techniques derived from our analysis to diminish vibration transmission to sensitive components. This entails the utilization of vibration isolation mounts, damping materials, and strategic component placement to mitigate direct exposure to vibration sources. Simultaneously, we will perform design optimization aimed at curbing vibration generation at its root. This endeavor involves refining the geometry and material properties of components, optimizing mechanical system layouts, and minimizing structural resonances that can exacerbate vibration levels. Through these concerted efforts, we aim to enhance the vehicle's resilience to vibration-induced stress, ensuring a smoother and more reliable performance on the track.

Furthermore, the evaluation and enhancement of structural components are imperative to bolster safety, particularly at higher speeds. Rigorous assessments will be conducted to identify any weaknesses or vulnerabilities in the existing framework, followed by the implementation of appropriate measures to reinforce structural integrity and resilience. In our pursuit of optimizing performance and responsiveness, the integration of a load cell emerges as a pivotal step. This will provide real-time feedback on load distribution and dynamics, allowing for precise adjustments and fine-tuning to maximize efficiency and traction.

In the pursuit of optimizing safety and performance, we are equally committed to enhancing ergonomics. This entails improving accessibility to essential controls, including electrical buttons and mechanical levers. Our focus extends to facilitating smoother gear changes, precise throttle modulation, and seamless clutch engagement. By strategically repositioning and refining these components within the dyno, we aim to enhance the driver's comfort and control. Ensuring intuitive access to controls not only enhances the overall system engagement but reassures operators that they will not do anything wrong.

Subsequently, we will conduct driving simulations emulating the FSAE style to fine-tune our engines appropriately. These simulations encompass various maneuvers such as acceleration, braking, and cornering, replicating FSAE style racing conditions. By subjecting our engines to these scenarios, we can refine their performance characteristics and optimize tuning parameters accordingly. Through analysis of simulation data and iterative adjustments, we aim to ensure that

our engines deliver optimal power delivery, responsiveness, and reliability on the track. This approach enables us to tailor our engines to meet the exacting demands of competitive racing, ultimately enhancing our competitiveness and performance.

**Acknowledgements**

This endeavor owes its realization to the collective efforts of numerous individuals, and we extend heartfelt appreciation to those whose invaluable contributions have paved the way for its success. Dr. Pranaya Pokharel, our esteemed mentor, played a pivotal role in guiding us through this project. Recognition is also extended to Dr. Salim Azzouz, the Director of Senior Design, Dr. Raj Desai, Chair of the Engineering Department, and Mr. Jay Barnett, our Laboratory Technician, for their unwavering support. Additionally, we acknowledge the crucial roles played by Mr. Frank Bohuslav, our Machinist Technician, and Dr. Sarah Cobb, Interim Dean of McCoy School of Science, Mathematics and Engineering, along with Ms. Christina Miller, the Secretary for McCoy School of Engineering.

Special mention goes to Jaden Corbin, a dedicated member of Mustangs Racing, Kory Prather, the skilled Welder for Mustangs Racing, and Sharome Burton, the esteemed Team Captain of Mustangs Racing. We express gratitude to our colleagues and classmates who provided invaluable feedback, contributing significantly to the enhancement of our project. The collaborative spirit and support from each mentioned individual have been instrumental in bringing this project to fruition and also in its continuation.

We express our gratitude to former group members Trevon Antoine and Nedabiah Warner for their invaluable contributions to the project's advancement. Their willingness to offer guidance and share insights into decision-making processes greatly benefited our team. Mr. Antoine provided invaluable advice on engine behavior, while Mr. Warner's expertise was instrumental in wiring the engine, as he generously shared the wiring diagram he had successfully utilized previously. Their expertise and support contributed to the project's progress and success.

**References:**

[1] Pokharel, P., Antoine, T., Joseph, G., & Warner, N. (2024). Frame design and fabrication of Engine Dynamometers for FSAE cars. Journal of Innovative Ideas in Engineering and Technology (ISSN: 2563-3678), 1(1), 33-97.

[2] Shaha, S. S., Chaturvedia, S., & Agustin, S. A. (2021). Design, Development and Validation of Engine Dynamometer for FSAE. *Turkish Online Journal of Qualitative Inquiry*, *12*(6).

[3] Romandoni, N., Aminudin, A., Faizin, K. N., Puspitasari, I., Agus, A. T. S., & Aziz, A. (2021, March). Design of Water Brake Dynamometer. In Journal of Physics: Conference Series (Vol. 1845, No. 1, p. 012048). IOP Publishing.

[4] Motahari-Nezhad, M., & Jafari, S. M. (2023). Experimental and data driven measurement of engine dynamometer bearing lifespan using acoustic emission. Applied Acoustics, 210, 109460.

[5] Tóth-Nagy, C., Koller, T., & Perger, J. (2022). Implementation of vehicle simulation model in a modern dynamometer test environment. Cognitive Sustainability, 1(4), 27-32.

[6] What is a dynamometer?. Power Test Dynamometer. (n.d.-b). https://powertestdyno.com/what-is-a-dyno/. Accessed 27 Aug. 2023

[7] "Eddy currents and electromagnetic braking explained." *YouTube,* YouTube, 2018, March 14, www.youtube.com/watch?v=BIsKthqeKSo&t=2s

[8] Bhuyan, Satyam. "Electromagnetic Induction: Definition, Examples, & Applications." S*cience Facts*, 1 Feb. 2023, www.sciencefacts.net/electromagnetic-induction.html.

[9] benofer90. "Formula of Average Magnetic B Field Strength of Large Conductor." *Physics Forums: Science Discussion, Homework Help, Articles*, Physics Forums: Science Discussion, Homework Help, Articles, 16 Aug. 2015, www.physicsforums.com/threads/formula-of-average-magnetic-b-field-strength-of-large-conductor.827579/.

[10] "Eddy Currents", 7 Dec. 2022. https://www.sciencefacts.net/eddy-current.html

[11] Admin. "What Is Lenz's Law? - Definition, Formula, Applications, Experiments." *BYJUS*, BYJU'S, 29 Aug. 2022, www.byjus.com/physics/lenzs-law/.

[12] *YouTube*, YouTube, 5 Jan. 2015, https://www.youtube.com/watch?v=5FMoUEmSsdE. Accessed 4 Dec. 2023.

[13] *Welcome to Telma USA*, www.telmausa.com/Downloads/TL136000.pdf. Accessed 5 Dec. 2023.

[14] *Welcome to Telma USA*, www.telmausa.com/Downloads/TL101018.pdf Accessed 5 Dec. 2023.

[15] *AF50-90 Light Vehicle Retarder - Telma USA*, www.telmausa.com/Downloads/OC141784.pdf. Accessed 5 Dec. 2023.

[16] *TL113040 Installation Manual for Telma AF50-90 on Ford F550 CAB Chassis ...*, www.telmausa.com/Downloads/TL113040.pdf. Accessed 5 Dec. 2023.

[17] "Eddy current retarder help. All About Circuits." Rocketman12. (2023, September 12). https://forum.allaboutcircuits.com/threads/eddy-current-retarder-help.186406/

[18] Singh, R. (n.d.). *Design of Shafts*. Machine Tool Lab. https://www.me.iitb.ac.in/~ramesh/courses/ME423/me423.html

[19] Budynas, R., Nisbett, K., (2019). *Shigley's Mechanical Engineering Design.* McGraw-Hill Education; 11th edition. ISBN: 978-1260569995.

[20] "Flange Couplings: Definition, Types, Advantages and Disadvantages." Testbook, testbook.com/mechanical-engineering/flange-couplings-definition#:~:text=The%20advantages%20of%20flange%20couplings%20include%"20reliable%20shaft%20connection%2C%20high,resistance%20to%20vibration%20and%20misalignment. Accessed 19 Sept. 2023.

[21] "Everything You Need to Know about Shaft Collars." *Acorn Industrial Services Limited*, www.acorn-ind.co.uk/insight/everything-you-need-to-know-about-shaft-collars/#:~:text=The%20main%20function%20of%20a,machine%20components%20on%20the%20shaft. Accessed 21 Oct. 2023.

[22] "7 Reasons Why Shaft Collars Fail." *Ruland Manufacturing*, www.ruland.com/technical-article-why-shaft-collars-fail. Accessed 21 Oct. 2023.

[23] Double universal joints - huco. (n.d.). https://www.huco.com/shop/power-transmission/steel-universal-joints/double-universal-joints

[24] "Power inverters explained - how do they work working principle igbt." YouTube. (2020, April 7). YouTube. https://www.youtube.com/watch?v=iIqhAX0I7lI

[25] Pokharel, P., Rowland, J., Snyder, T., & Gonzalez, L. (2022, October). Innovations for Clutching and Shifting in Formula-Style Drivetrains. In ASME International Mechanical Engineering Congress and Exposition (Vol. 86694, p. V007T09A018). American Society of Mechanical Engineers.

[26] Omega LC103B-100 S BEAM LOAD CELL, 21 Nov. 2023

[27] *LC103B-100 - s beam load cell, 100lb, 12VDC*. Newark. (n.d.). https://www.newark.com/omega/lc103b-100/s-beam-load-cell-100lb-12vdc/dp/32AH7796?st=100lb+s+type+load+cell